ADB

Technical Assistance Consultant's Report

Project No: 42384-012
April 2020

Knowledge and Innovation Support for ADB's Water Financing Program

Water Productivity and Water Accounting Methodology Manual

Prepared by

IHE Delft Institute for Water Education and the International Water Management Institute

For Asian Development Bank

ASIAN DEVELOPMENT BANK

Water Productivity and Water Accounting Methodology Manual

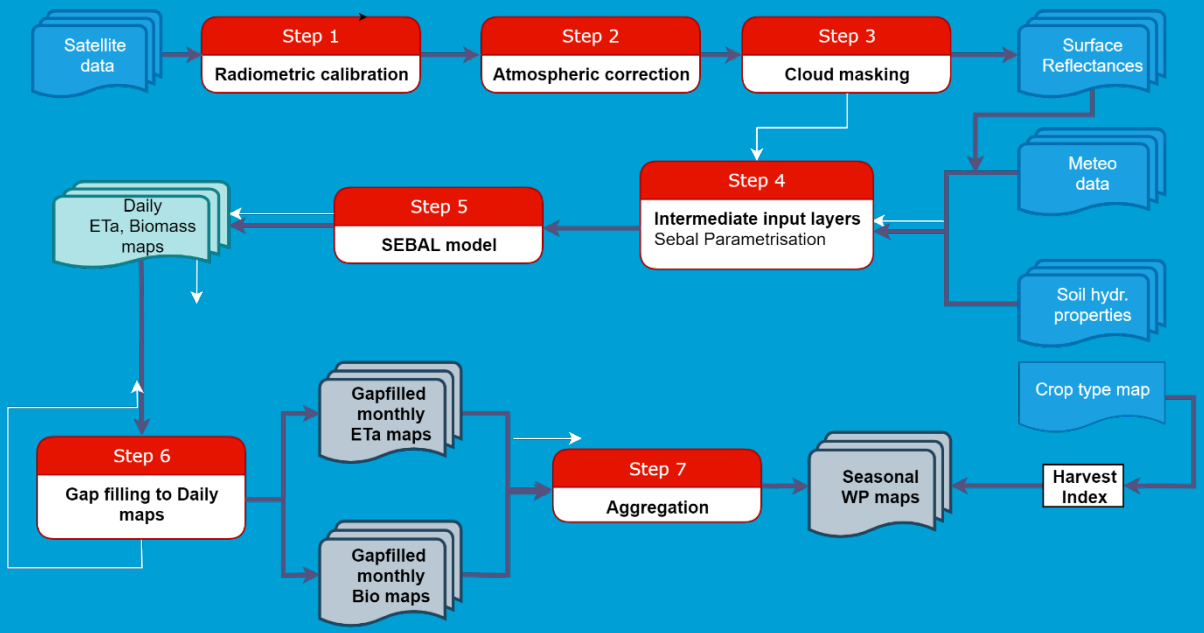

UNESCO IHE DELFT

ADB

IWMI International Water Management Institute

Project final report submitted to the Asian Development Bank under the program for Expanding support to Water Accounting in River Basins and Water Productivity in Irrigation Schemes. The designations employed and the presentation of material in this information product do not imply the expression of any opinion whatsoever on the part of the Asian Development Bank (ADB) or IHE Delft Institute for Water Education (IHE DELFT) or the International Water Management Institute (IWMI) concerning the legal or development status of any country, territory, city or area or of its authorities, or concerning the delimitation of its frontiers or boundaries. The mention of specific companies or products of manufacturers, whether or not these have been patented, does not imply that these have been endorsed or recommended by ADB or IHE DELFT or IWMI in preference to others of a similar nature that are not mentioned. The views expressed in this information product are those of the author(s) and do not necessarily reflect the views or policies of ADB or IHE DELFT or IWMI.

Citation: Mul, M., Karimi, P., Coerver, H.M., Pareeth, S., Rebelo, L.M., 2020. Water Productivity and Water Accounting Methodology Manual. Project report, IHE Delft Institute for Water Education, The Netherlands and the International Water Management Institute, Sri Lanka.

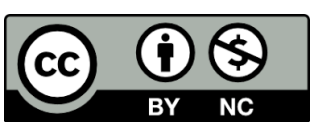

EXPANDING SUPPORT TO WATER ACCOUNTING IN RIVER BASINS AND WATER PRODUCTIVITY IN IRRIGATION SCHEMES

Project report:

Water Productivity and Water Accounting Methodology Manual

PREPARED FOR THE
ASIAN DEVELOPMENT BANK
BY

IHE Delft Institute for Water Education
and
International Water Management Institute

April 2020

List of abbreviations

ADB	Asian Development Bank
AGBP	Above Ground Biomass Production
APAR	Absorbed Photosynthetically Active Radiation
AR	Autotrophic Respiration
CV	Coefficient of Variation
CWP	Crop Water Productivity
DEM	Digital Elevation Model
DN	Digital Number
DOS	Dark Object Subtraction
dT	Difference in temperature
EF	Evaporative Fraction
EO	Earth Observation
EOS	End of the Season
ESA	European Space Agency
ET_a	Actual Evapotranspiration
EWSIP	Enhanced Water Security Investment Program
f	Above Ground Fraction
FAO	Food and Agriculture Organization
G	Ground Heat Flux
GLDAS	Global Land Data Assimilation System
GPP	Gross Primary Production
GRACE	Gravity Recovery and Climate Experience
GRanD	Global Reservoir and Dams database
H	Sensible Heat Flux
HI	Harvest Index
I	Incoming water flows
IHE Delft	IHE Delft Institute for Water Education
IWMI	International Water Management Institute
LAI	Leaf Area Index
LE	Latent Heat Flux
LUE	Light Use Efficiency
LULC	Land-use/ Land-cover
LWR	Locally Weighted Regression
MLU	Managed Land Use
MODIS	Moderate Resolution Imaging Spectroradiometer
MWSIP	Mahaweli Water Security Investment Program
MWU	Managed Water Use
NASA	National Aeronautics and Space Administration
NDVI	Normalized difference vegetation index
NIR	Near Infra-Red
NPP	Net Primary Production
O	Outgoing water flows
P	Precipitation

PLU	Protected Land Use
pySEBAL	Python implementation of SEBAL
Q_{desal}	Flows into the basin from desalinated water
Q_{gw}^{in}	Flows into the basin from groundwater
Q_{sw}^{in}	Flows into the basin from surface water
Q_{sro}	Surface runoff
R	Recharge
r	Runoff Ratio
Rh	Relative Humidity
Rn	Net Radiation
RS	Remote Sensing
SAVI	Soil Adjusted Vegetation Index
SD	Standard Deviation
SDG	Sustainable Development Goal
SEBAL	Surface Energy Balance Model
SOS	Start of the Season
SRTM	Shuttle Radar Topography Mission
SWI	Soil-Water-Index
SWIR	Short Wave Infra-red
TA	Technical Assistance
TIR	Thermal Infra-red
TOA	Top of Atmosphere
ULU	Utilised Land Use
WA+	Water Accounting Plus
WP	Water Productivity
$\Delta S/\Delta t$	Storage Change
θ	Moisture Content
θ_{sat}	Saturated Water Content

Table of Contents

Table of Figures

Table of Tables

I. Introduction

1. The Asian Development Bank (ADB) is committed under its Water Operational Plan 2011-2020 to undertake expanded and enhanced analytical work to enable its developing member countries to secure deeper and sharper understanding of water issues and solutions. IHE Delft, in collaboration with IWMI and FAO, supports ADB in achieving this objective.

2. The activities proposed for the current Technical Assistance (TA) build on the work previously undertaken by IHE Delft in cooperation with the ADB to assess crop water productivity and to assess water resource status in selected basins/countries in Asia.

3. Assistance will be provided to projects in 7 countries; Cambodia, India, Indonesia, Kazakhstan, Mongolia, Philippines, and Sri Lanka. In India, Kazakhstan, Mongolia, Philippines and Sri Lanka this takes the form of water accounting assessments to characterize water use and availability, while in Cambodia, India, Indonesia and Kazakhstan emphasis is being placed on water productivity or irrigation performance assessments, to target investment.

4. This document explains how the mentioned assessments of the crop water productivity and the water resources status through water accounting in selected basins/ countries in Asia will be carried out. The first part of the report is dedicated to water productivity assessment, while the second part elaborates on methods used for water accounting in general and Water Accounting Plus in particular.

II. Water Productivity

A. What is Water Productivity

5. Water productivity (WP) measures the ability of a water system to convert units of water use to products and services (Molden, 1997). It is defined as the ratio of net benefits from any ecosystem services such as forestry, fishery, livestock, and crops to the amount of water required to produce those benefits. It thus reflects the idea of getting more benefits while using less water.

6. When WP is measured specifically for crops, it is also called Crop Water Productivity (CWP). WP can be further divided into two major types:

- Physical WP is the ratio of the mass of agricultural output to the amount of water used.
- Economical WP is the ratio of the financial value obtained per unit of water used.

7. WP is a performance indicator that can be used for monitoring, evaluating, and diagnosing agricultural water management practices. It aims to integrate the productivity of the use of land and water resources. Since food security remains the primary goal of the agricultural sector, measures to limit water consumption in agriculture should not come at the cost of curbing food production.

8. Hence, improving WP is gaining attention because it can be a useful tool in addressing the issue of increasing food demand with increasing water limitations. This has been recognised by the United Nations Sustainable Development Goals (SDGs) which stipulate that agricultural productivity should be doubled by 2030 (SDG 2.3) and that water use efficiency must be substantially increased (SDG 6.4).

B. Importance of Water Productivity

9. The gap between food production and food demand is increasing in many countries. While this is mainly related to population growth and changing diets, there is also the issue of insufficient water resources being available to produce large amounts of food required. Food production consumes a significant amount of water, ranging from 4,000 to 12,000 m^3/ha/season, and for certain tropical fruit crops, this can even reach 22,000 m^3/ha/season.

10. Hence there is an increasing call to produce the same amount of food with less water, or when feasible, produce more food from less water resources ("*more from less*"). The key performance indicator to monitor this is WP ("*more crop per drop*"). Increasing WP leads to increases in crop yields and/or decreases in crop water use. WP is a relative indicator and increasing WP does not necessarily mean better performance.

11. For example, WP of rainfed agriculture could be higher than that of irrigated agriculture while the rainfed yields are almost always less than irrigated agriculture. Hence, WP must be seen in relation to the overall availability of water resources and should be prioritized when water saving in agriculture is the desired outcome due to an existing shortage of water across space and over the duration of a crop growing season. An assessment of the performance of agricultural water management in ten international river basins across Asia, Africa, and Latin America found

vast differences in the WP (Cai et al., 2011). The spatial and temporal differences in WP show the underlying variation in yields and water consumption which in turn is highly dependent on the local conditions.

12. The WP concept is developed in recognition of the constraints with traditional irrigation efficiency indicators. These traditional indicators focus heavily on the engineering aspects of irrigation, which has a bias towards infrastructure investments (such as canal lining).

13. WP, however, does not capture water reuse in a system and the ability of irrigation systems to turn water supply into food production. Neither does it reflect the competitive demand from outside the agriculture sector at a larger scale. Figure 1 shows that irrigation efficiency in effect represents only a small portion of hydrological processes in a farming system. Irrigation efficiency is not addressing the concepts of consumptive use from the viewpoint of total water resources available.

14. Irrigation efficiency merely looks at water from sources to the field from a “supplier” point of view. Farmers are more interested in the results of irrigation (e.g. nutrition, income, jobs) rather than on how efficient that production is acquired. Food production is more essential for them, and if water is the major input constraint to food production, it makes sense to express it per unit of water consumed. This philosophy is now widely accepted and adopted in the international community, including donor agencies.

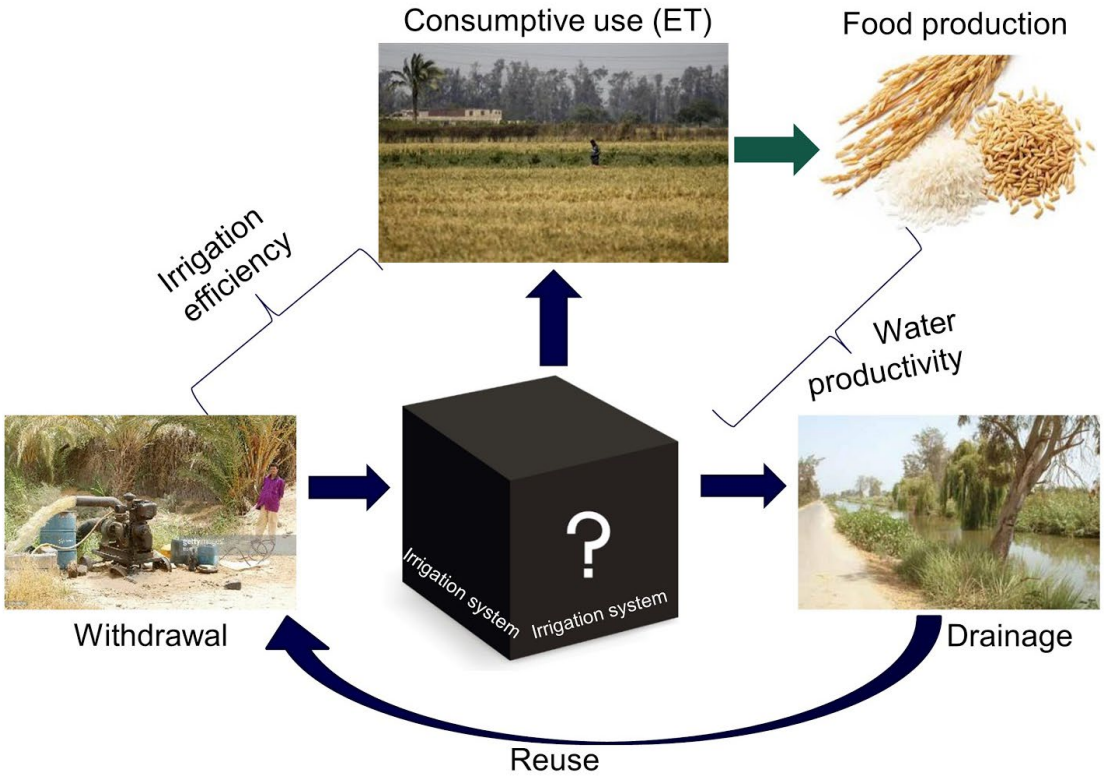

Figure 1 - Irrigation efficiency and water productivity indicators for irrigation systems. The two indicators are complementary while WP covers more advanced and broader components of irrigation performance.

15. WP indicators are broader than irrigation efficiency indicators. As shown above, WP does not replace irrigation efficiency. Rather it brings two major outcomes of irrigation water management into one single expression; crop production, the purpose of farming and irrigation; and the water consumed, the means to achieve the production. In achieving higher WP, it is still

important to look at field level application efficiency, and cross-sector, upstream/downstream allocative efficiency at the river basin level.

16. WP was originally an agronomy term to measure plant water use efficiency. It was revised and given a new definition to represent the ability of a system to convert water consumed into goods and services (Molden, 1997). WP is a significant step forward in linking water management with broader policy goals such as water security, food security, and economic development. Kilograms of fresh food can be converted into gross returns ($), employment (jobs), nutrition (calories). Reducing the consumptive use enables more water to remain in the physical system for allocation to other sources. WP benchmarking links water managers with development target settings and investment strategies.

17. Although improving WP can indeed contribute to the solution to combat the water and food crisis, in reality, it is more difficult to achieve WP improvements at the farm level, partially because target values are absent and farmers/irrigators are not guided by any means. They often associate water savings with lower amounts of applied water, fewer irrigation turns, or a higher on-farm irrigation efficiency, and are not concerned with the consumptive use of irrigation water and the production that is associated with that.

C. Water Productivity using Remote Sensing

18. Water productivity of agricultural activities can be quantified on the basis of crop yield harvested and net water consumed.

19. Remote sensing (RS) based assessment of WP focuses on actual evapotranspiration (ET_a) to estimate net water consumption. The term Evapotranspiration combines the two different processes of evaporation and transpiration. Both these processes relate to the removal of vaporised liquid water from the earth's surface to the atmosphere. Evaporation happens from surfaces such as water bodies, rivers, soils, wet leaves, and pavements. Transpiration occurs through plants by the passage of water through the opening of the plant's stomatal pores into the atmosphere.

20. When crop growth and production are concerned, transpiration is considered as a beneficial consumption, and evaporation from soil/water and canopy interception, a non-beneficial consumption (Figure 2). The reason is that, among the two, it is only transpiration that contributes to biomass growth. The WP is estimated on a seasonal basis and the ET_a is taken as the accumulated crop ET_a, from the start of the season (SOS) until the end of the season (EOS).

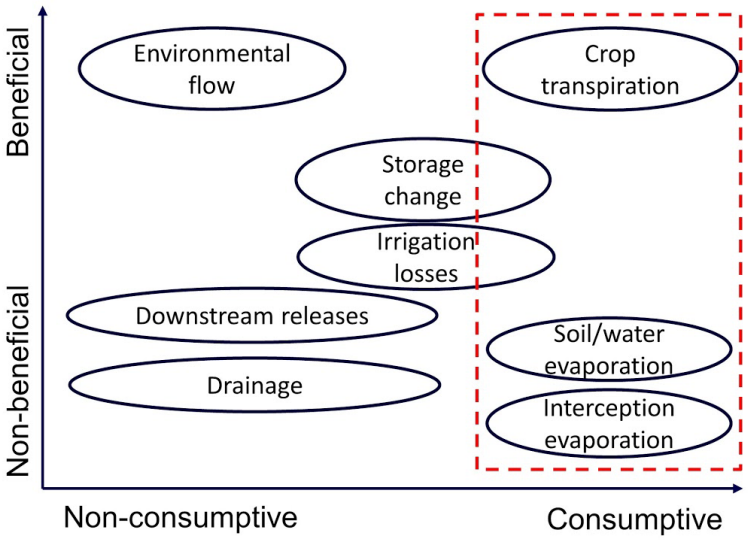

Figure 2 - Remote sensing-based WP approach focuses on the beneficial and non-beneficial consumptive use of water.

21. The remote sensing-based estimates of biomass production, and subsequently crop yield, is primarily based on the relationship between the absorbed light and carbon assimilation by the plant. This relationship in most plants is relatively constant. This ratio, termed light use efficiency (LUE), is used to convert remote sensing-based estimations of light absorption to gross primary production (GPP).

22. Consequently, the net primary production (NPP) is calculated after subtraction of carbon lost to autotrophic respiration (AR) from GPP. NPP is then used to estimate dry biomass production using a conversion factor from organic carbon to dry organic biomass.

23. The final step is, then, the calculation of crop yield which is done using the harvest index (HI), above ground fraction (f) and the moisture content (θ) of the harvest. The HI definition varies from one crop to another. For instance, HI for cereals is defined as the ratio of grain yield to total seasonal above-ground biomass, and for potato, it is defined as the ratio of tuber to total seasonal biomass production.

D. Surface Energy Balance modelling

24. The Surface Energy Balance Model (SEBAL), is a single-source model that uses visible, near-infrared and thermal infrared data collected mainly by sensors onboard earth observation satellites (Bastiaanssen et al., 1998). The model estimates ET_a from the residual of the energy balance (i.e. latent energy (LE)) by computing the net incoming radiation (R_n), sensible heat flux (H) and Soil heat flux (G) per image pixel as shown in Eq. (1).

$$LE = R_n - G - H \quad (1)$$

25. LE is converted into ET, expressed as a depth of water per time, dividing by the latent heat of vaporization and a correction for the density of water. Once LE is computed, an equivalent amount of instantaneous ET (mm/s) is readily calculated by dividing by the latent heat of vaporization (L) and the water density (ρ_w) (Eq. (2)):

$$ET = \frac{LE}{L * \rho_w} \quad (2)$$

26. Optical sensors in Earth Observation (EO) satellites measure spectral radiances in different wavelengths of the electromagnetic spectrum. The data from Landsat satellites (4, 5, 7 and 8) and MODIS sensor onboard Aqua and Terra satellites by NASA are commonly used for ETa mapping due to the availability of thermal radiances. Data from recent Sentinel (2 and 3) missions by ESA are also now being used for similar studies. The availability of these datasets in the public domain (see https://earthexplorer.usgs.gov/ and https://scihub.copernicus.eu/) helps to popularise these applications of remote sensing. The emitted and reflected energy indicates the spectral properties of the objects which then can be related to biophysical properties. Thus we are able to monitor processes like evapotranspiration which is strongly influenced by the thermal property of the object in the ground.

27. The spectral radiance measurements by the satellites are stored often in rasters which are represented by a set of pixels. Every pixel represents a value for a unit area size which depends on the sensor properties. For instance, Landsat-satellites provide images with pixel areas of 30x30 m^2 while Proba-V has a pixel size of 100x100 m^2. The underlying principle of the use of surface energy balance models to estimate ET_a is that the total incoming solar energy is equal to the total energy reflected back into the atmosphere and the consumed energy. The component of consumed energy is also referred to as the latent heat flux which represents energy that is consumed to vaporize water through both processes of transpiration and evaporation (see Figure 3). The latent heat flux over a vegetated surface (for example an agriculture area) lowers the surface temperature and this change over time is related to evapotranspiration. Hence by solving the energy balance equation, the amount of energy used for vaporizing water becomes known and that can be converted to a volume of water that is evaporated (either through evaporation or transpiration).

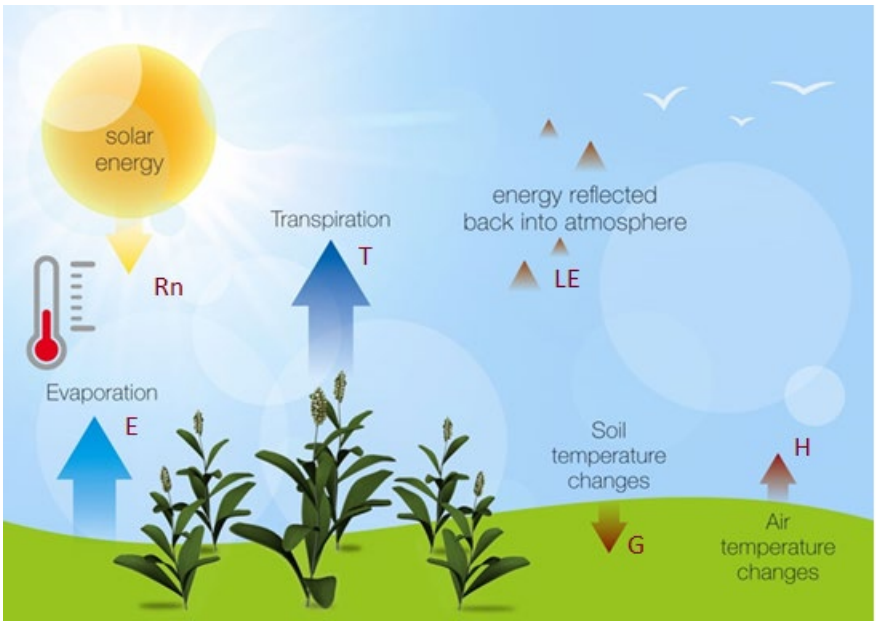

Figure 3 - Schematic view of the energy balance principle.

28. SEBAL is used as the standard tool to calculate ET_a, biomass production and WP due to its robustness and high level of accuracy (Karimi and Bastiaanssen, 2015). PySEBAL, developed by IHE Delft, is a new python implementation of the SEBAL model.

29. PySEBAL is a python library where a set of input data including spectral, atmospheric, soil and topographic data are used as input to estimate the surface energy balance components. The outputs include parameters related to vegetation, energy balance, biomass, evapotranspiration, and water productivity. The PySEBAL library is provided as an open-source library with Apache version 2 license in a GitHub repository (https://github.com/wateraccounting/SEBAL).

30. The python implementation facilitates automation of the entire process including the estimation of the hot and cold pixels from a satellite image (Figure 4). These hot and cold pixels are known as “anchor”-pixels and are needed to compute the representational difference in temperature between two near-surface heights of the region under study (dT), which is one of the key parameters for SEBAL. The cold pixels in SEBAL are usually selected from water bodies or crop areas with well-developed vegetation, whereas hot pixels are selected from completely dry soil surfaces. In PySEBAL cold pixels are automatically identified using the distribution of surface temperature estimated from the Landsat thermal data, while hot pixels are identified using the distribution of NDVI.

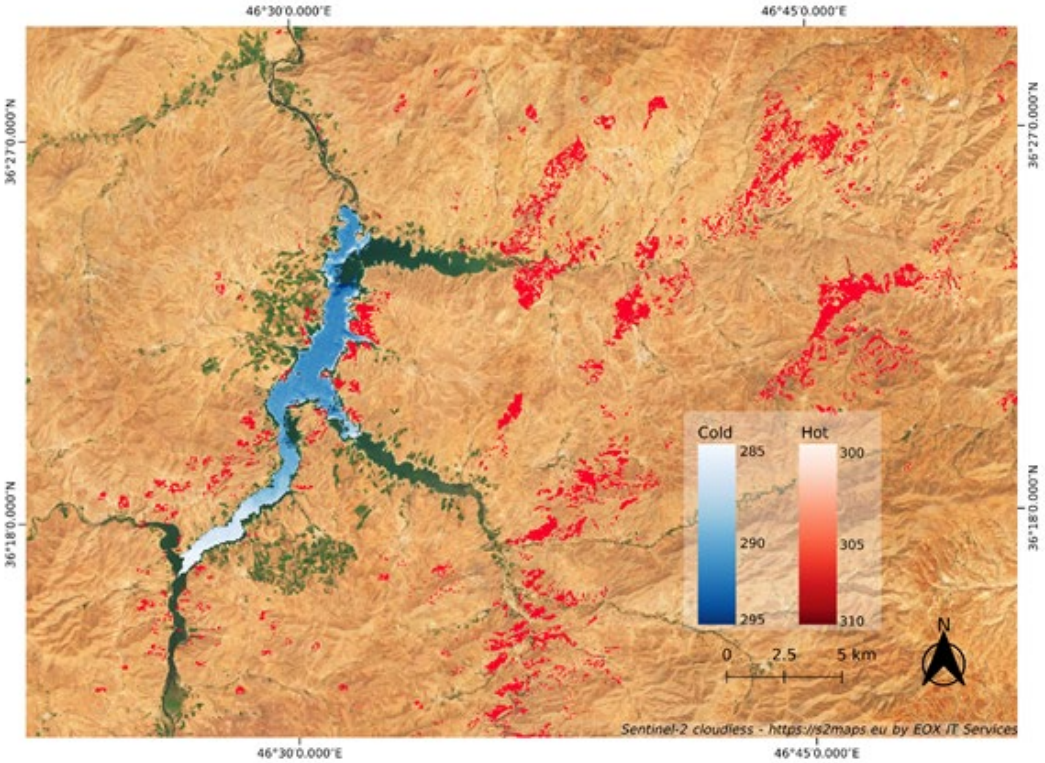

Figure 4 - Cold and Hot pixels automatically detected by pySEBAL on Landsat 8 image acquired on 7 Dec 2015 in Urmia basin, Iran; Cold pixels are located over a reservoir and hot pixels over drylands.

31. Currently, PySEBAL supports data from MODIS, Landsat, and Proba-V satellite sensors which facilitate the production of daily ET_a and seasonal WP maps. PySEBAL also supports the secondary data in a spatial format or as a numeric input (Table 1). Figure 5 shows the workflow of computing daily ET_a and WP using PySEBAL.

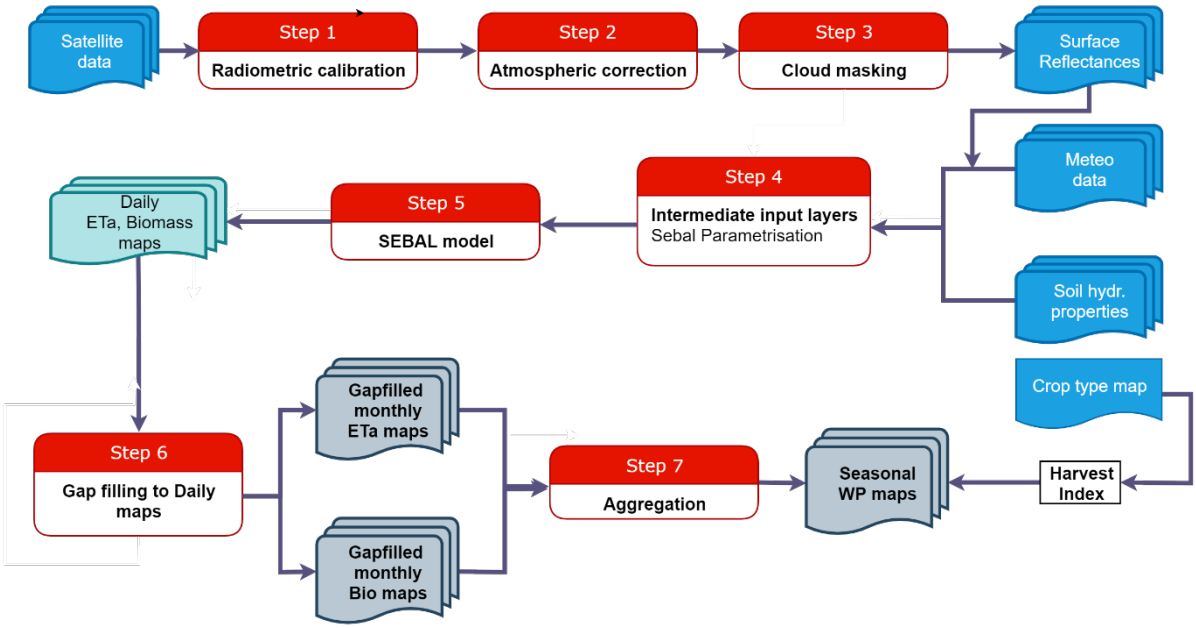

Figure 5 - The PySEBAL methodological framework for WP assessment.

32. The implemented method in PySEBAL includes pre-processing of the satellite data, including radiometric calibration, atmospheric correction using Dark Object Subtraction (DOS) method and cloud/water pixel masking (steps 1 to 3 in Figure 5). The radiometric calibration converts Digital Number (DN) to Top of Atmosphere (TOA) spectral reflectances (step 1), atmospheric correction further converts TOA radiance into surface reflectance (step 2). In step 3, the cloud pixels are removed using the quality assessment layers provided with the satellite data.

33. Step 4 is to create intermediate input layers that are required for closing energy balance equation and biomass production. These intermediate inputs includes layers of data and information on vegetation, climate and soil. Examples are the Normalized Difference Vegetation Index (NDVI), Soil-Adjusted Vegetation Index (SAVI), Leaf Area Index (LAI) and Albedo. The vegetation indices calculated are used to compute thermal emissivity, vegetation cover and vegetation properties like displacement height. LAI is also used to compute surface resistance. Albedo is used to compute radiation parameters like extra-terrestrial radiation, net radiation, and soil heat flux.

34. Step 5 computes the energy balance components the R_n, G, and H. R_n represents the actual radiant energy available at the surface. It is computed by subtracting all outgoing radiant fluxes from all incoming radiant fluxes as shown in Eq. (3).

$$R_n = R_s^{\downarrow} - \alpha | * R_s^{\downarrow} + R_L^{\downarrow} - R_L^{\uparrow} - (1 - \varepsilon_0) * R_L^{\downarrow} \quad (3)$$

35. Where $R_s^{\downarrow}$ is the incoming shortwave radiation (W/m^2), α is the surface albedo (dimensionless), $R_L^{\downarrow}$ is the incoming longwave radiation (W/m^2), $R_L^{\uparrow}$ is the emitted outgoing longwave radiation (W/m^2), and ε_0 is the surface thermal emissivity (dimensionless). The final term, $(1-\varepsilon_0)R_L^{\downarrow}$, represents the fraction of incoming longwave radiation that is reflected from the surface (see Figure 28).

36. The soil heat flux (G) is empirically calculated using vegetation indices, surface temperature, and surface albedo. Soil heat flux is the rate of heat storage into the soil and vegetation due to conduction. Soil heat flux is the rate of heat storage into the soil and vegetation due to conduction. The ratio G/R_n can be estimated using the following empirical equation, Eq. (4) representing values near midday:

$$G/R_n = T_s * (0.0038 + 0.0074 * \alpha) * (1 - 0.98 * NDVI^4) \quad (4)$$

37. Where T_s is the surface temperature (°C), α is the surface albedo, and NDVI is the Normalized Difference Vegetation Index. G is then calculated by multiplying G/R_n by the value for R_n. Sensible heat flux (H) is the rate of heat loss to the air by convection and conduction, due to a temperature difference. It is computed using a one-dimensional, aerodynamic, temperature gradient based equation for heat transport (Eq. (5)).

$$H = \frac{\rho_a * c_p * dT}{r_{ah}} \quad (5)$$

38. Where: ρ_a is air density (kg/m^3), c_p is air specific heat (1,004 J/kg/K), dT (K) is the vertical air temperature difference ($T_1 - T_2$) between two heights (z_1 and z_2), and r_{ah} is the aerodynamic resistance to heat transport (s/m).

39. For sensible heat flux (H), one of the key parameters required is dT, which is near-surface air temperature difference for each pixel. As the actual absolute values for air temperatures above each pixel are unknown, dT is computed by assuming a linear relationship as shown in Eq. (6) between dT and DEM corrected surface temperature. To define the slope and offset of this linear model, SEBAL uses the two “anchor” pixels where a value for H can be reliably estimated. For each satellite image, these “anchor” pixels are selected by picking hot and cold pixels over the driest surface in the satellite scene and water body respectively.

$$dT = a * T_s^{dem} + b \quad (6)$$

40. Where b and a are the calibration coefficients, and T_s^{dem} is surface temperature from the satellite ‘delapsed’ adjusted to a common sea level datum using a specified lapse rate. The adjustment to T_s compensates for the change in T_s with an elevation that is related more to warming or cooling of air masses with the change in elevation rather than with a change in surface energy balance and evaporation.

41. The instantaneous Latent Heat Flux (LE) and Evaporative Fraction (EF) at the time of satellite data acquisition is then computed from the energy balance components. The instantaneous EF is then converted to daily ET_a for the day of satellite data acquisition by assuming the marginal difference between instantaneous EF and EF derived from the 24-hour energy balance (Eq. 34 in Appendix A).

42. The daily ET_a computed from multiple satellite overpass dates over a season is then gap-filled and aggregated to create seasonal maps. A vegetation index-based approach using Absorbed Photosynthetically Active Radiation (APAR) and Light Use Efficiency (LUE) is applied to compute (Eq. (7)) daily Above Ground Biomass Production (AGBP) maps followed by gap-filling and aggregation to produce seasonal maps.

$$AGBP = APAR * LUE \quad (7)$$

43. Where AGBP is Above Ground Biomass Production in kg/ha. Steps 6 and 7 are the post-processing part of the methodology where gaps due to cloud cover are filled to create gap-free daily maps and aggregated to seasonal/annual maps. For every month, Landsat has 4 observations, two from Landsat 7 and two from Landsat 8, 16 days being the re-visit time of both satellites. But often cloud cover creates considerable gaps leading to null pixels. A gap-filling approach using Local Weighted Regression (LWR) to temporally fill the gaps for every 4 months at a time followed by a spline-based spatial interpolation is deployed to develop gap-filled monthly maps. The temporal gap-filling calculates missing values and outliers. For each time series observation (pixel) in the map, a polynomial model is computed using a set of neighbouring pixels in the time dimension. Then this model is applied to the respective time frame to estimate the values. Distance-based weight is applied to the values in such a way that the observation farther away in time gets lower weights. All the observations in the time series are interpolated, as long as there were enough non-null observations. The remaining gaps due to insufficient valid observations in the time series meeting the LWR conditions are then reconstructed using bicubic spline interpolation applied spatially.This step is applied only to the NULL pixels computing from the neighbouring valid pixels, which means the observations and temporally interpolated estimates will remain unchanged.

44. Yield and WP is then computed using the formula given in the Eq. (8) and Eq. (9) respectively.

$$Yield = HI * AGBP \quad (8)$$

$$WP(kg/m^3) = \frac{Yield(kg/ha)}{Water\ use(m^3/ha)} \quad (9)$$

45. A detailed explanation of the SEBAL implementation with equations is provided in Appendix A.

46. The objectives and justification of the steps explained above are presented in the matrix in Figure 6. The entire processing framework is divided into five major components as shown in the columns of the process matrix. Each component has distinct objectives and outputs which are interlinked and interdependent. In the first two components of pre-processing and calibration, the input data are processed to derive parameters and thresholds needed for the PySEBAL model followed by the step of computation with the major outputs, i.e. energy balance components, biophysical parameters, ET_a, and biomass, etc. In gap-filling an advanced statistical approach is used to fill the data gaps that may be present due to clouds or missing observations. In the final step of the assessment, the daily maps are aggregated to seasonal/annual scale and WP is computed based on a land-use/crop type map obtained from a secondary source. In this process matrix, the post-processing part of gap-filling and assessment is done outside the PySEBAL framework. For better understanding, each column in Figure 6 is linked to steps in Figure 5 explaining the methods implemented.

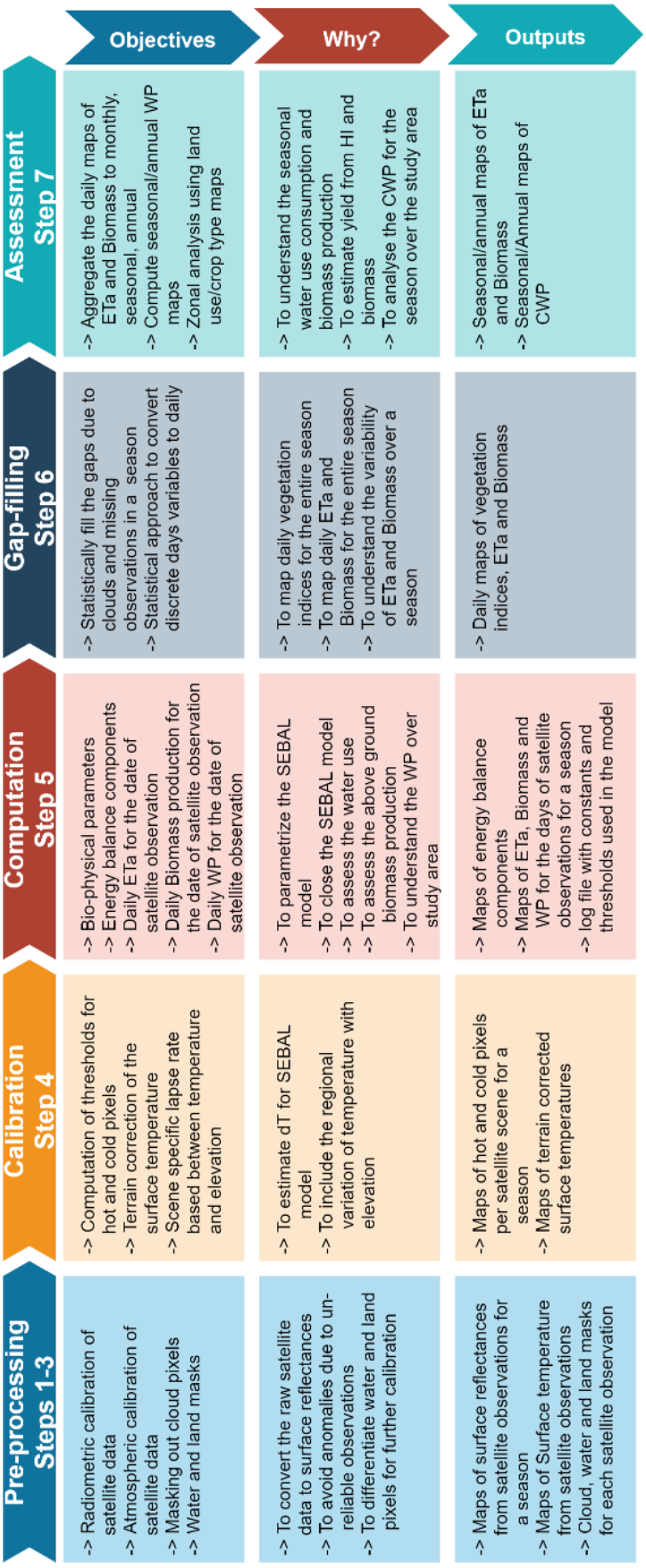

Figure 6 - Process matrix of the PySEBAL for WP assessment. Please refer to Figure 5 for the methodological framework linking steps given in the header.

47. The opportunity to the use high-resolution satellite imagery such as Landsat 8 for ET_a and WP calculation allows the users to extract key information on the use and productivity of water across multiple management scales from basin and irrigation scheme to blocks and fields. Figure 7 shows the seasonal ET_a over an irrigation block in Miandoab irrigation scheme in Iran. The map is produced by PySEBAL using Landsat 7 and 8 imagery with a spatial resolution of 30 meters by 30 meters. It shows how PySEBAL is capable of capturing variation in ET_a from one field to another. In doing so, it enables the users to extract field-specific information on water use and productivity that can be used to analyse the difference and come up with possible field specific attributes.

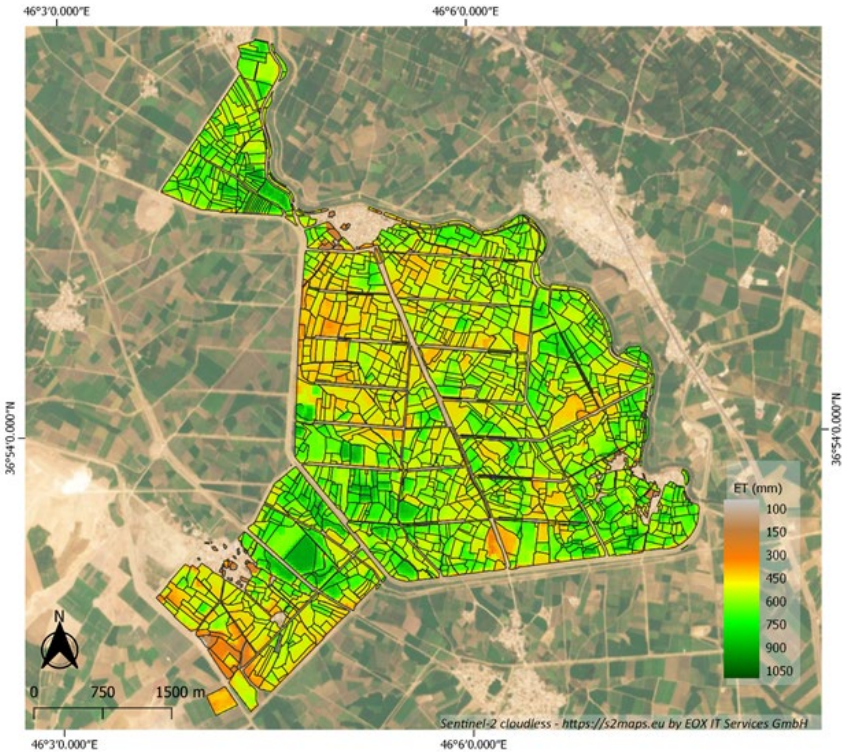

Figure 7 - Example PySEBAL output of seasonal ETa produced using Landsat 7 & 8 images, the case of Urmia, Iran.

1. Data requirements for PySEBAL

48. Major inputs to PySEBAL are satellite observations over various wavelengths of the spectrum. SEBAL requires surface temperature and air temperature at 2m height to compute LE and EF. Thermal data obtained and corrected to altitude is used for surface temperature and air temperature is obtained from meteorological stations or other secondary sources. Thus PySEBAL can support all satellite data as long as they offer data in visible, near-infrared, shortwave infrared and thermal infrared. It can read secondary data such as meteorological and soil variables in numeric as well as in spatial formats.

49. The PySEBAL is capable of processing multiple satellite scenes in a single run. The optimal way is to set up and run PySEBAL for an entire season at one go. Then the outputs are computed for every date of the satellite data in a season; assuming data is available in all scheduled observation dates, with MODIS outputs being available at daily intervals with a 250m resolution and with Landsat data being available every 8/16 days at a 30m spatial resolution. For each available date, the meteorological data as listed in Table 1 have to be prepared in two sets. The first set of data will represent the instantaneous observation of the meteorological variables

at the time of satellite data acquisition (for example 10:30 AM local time for Landsat) and the second set will be the daily average of the meteorological variables for the day of satellite data acquisition. Depending on the size and heterogeneity of the study area, meteorological data can be obtained from single or multiple stations within the study area. If the data is from a single station, the meteorological input is prepared as numeric values, whereas if the data is coming from multiple stations well distributed in the study area, the meteorological parameters will be interpolated to a spatial map which will then be read by PySEBAL. In the absence of station data from the study area, global spatial datasets like GLDAS and ERA5 can be used as inputs. Soil hydraulic properties and digital elevation model (DEM) are single observations for a study area as they are static properties. DEM is often retrieved from the Shuttle Radar Topography Mission (SRTM) which is an international platform that obtained digital elevation models at 30m spatial resolution. The soil hydraulic properties are either from field observations or secondary sources. In the absence of field observed soil hydraulic properties, we use data from a global database called HiHydroSoil (https://www.futurewater.eu/2015/07/soil-hydraulic-properties/) as inputs. Table 1 details all the input data required for PySEBAL for conducting remote sensing WP analysis.

Table 1 - An overview of the most important datasets used to estimate WP using remote sensing.

Variable	Parameter	Unit	Description
		Satellite data	
Visible	R,G,B	-	Spectral reflectances from satellite sensors like Landsat, MODIS, Proba-V from the visible spectrum.
Near-infrared	NIR	-	Spectral reflectances from satellite sensors like Landsat, MODIS, Proba-V from the NIR spectrum.
Short wave infrared	SWIR	-	Spectral reflectances from satellite sensors like Landsat, MODIS, Proba-V from the SWIR spectrum.
Thermal infrared	TIR	K	Thermal data from satellite sensors like Landsat, MODIS, Proba-V from the TIR spectrum.
		Meteorological data	
Downward shortwave radiation	SW_{down}	W/m^2	Total amount of shortwave radiation (both direct and diffuse) that reaches the Earth's surface.
Wind speed	W_S	m/s	Wind speed at 2m height.
Air temperature	T_{air}	℃	Air temperature at 2m height.
Pressure	P	Mb	Air pressure at 2m height.
Relative humidity	Rh	%	The amount of water vapour present in air expressed as a percentage of the amount needed for saturation at the same temperature.
		Topography	
Digital Elevation Model	DEM	m	Height of the land surface above the mean sea level.
		Soil hydraulic properties	
Saturated water content	WC_{sat}	m^3/m^3	Saturated water content is the maximum amount of water a soil can store.

Residual water content	WC_{red}	m^3/m^3	Water content for which the gradient d(volumetric water content)/dh becomes zero. Further drying does not occur under natural conditions
Field capacity	WC_PF2	m^3/m^3	Field capacity is the amount of water content in the soil after excess water has drained away.
Wilting point	$WC_PF4.2$	m^3/m^3	Wilting point is defined as the minimum amount of water in the soil that the plant requires not to wilt.

E. Case Studies

1. Indonesia

50. The focus of the WP assessment study in Indonesia was selected sites in Bali, West Java, and Lombok. Remote sensing based analysis combined with fieldwork was conducted in Bali and West Java to support the WP mapping with 'ground truth' data. The ground truth data were collected from the fields using a smartphone-based survey of farmers and extension officers. This data, together with secondary data from local governmental institutes were used to verify the remote sensing outputs of yield and crop types.

51. The WP maps show high spatial variability in all study sites, which implies that field management practices and the performance levels are not uniform. The average WP of paddy rice was 1.1, 0.76 and 1.4 kg/m^3 for Bali, West Java and Lombok respectively. The consumptive use during the dry season was 506, 473 and 374 mm/season respectively. The paddy yield was 5.6, 3.6 and 5.0 ton/ha respectively. Bali thus has the highest water consumption and the highest rice yield per unit area. However, due to having higher seasonal ET_a, Bali with an average WP of 1.1 kg/m^3 performs worse than that of Lombok that has WP of 1.4 kg/m^3. The world-wide average value for WP for paddy rice is 1.1 kg/m^3. WP in Bali is very much comparable to this global benchmark value, while Lombok shows higher and West Java shows lower performances.

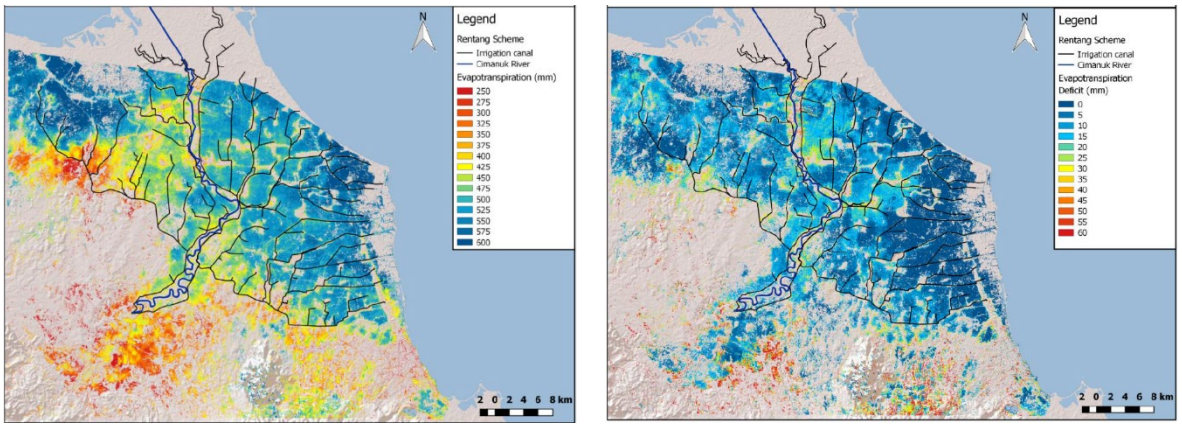

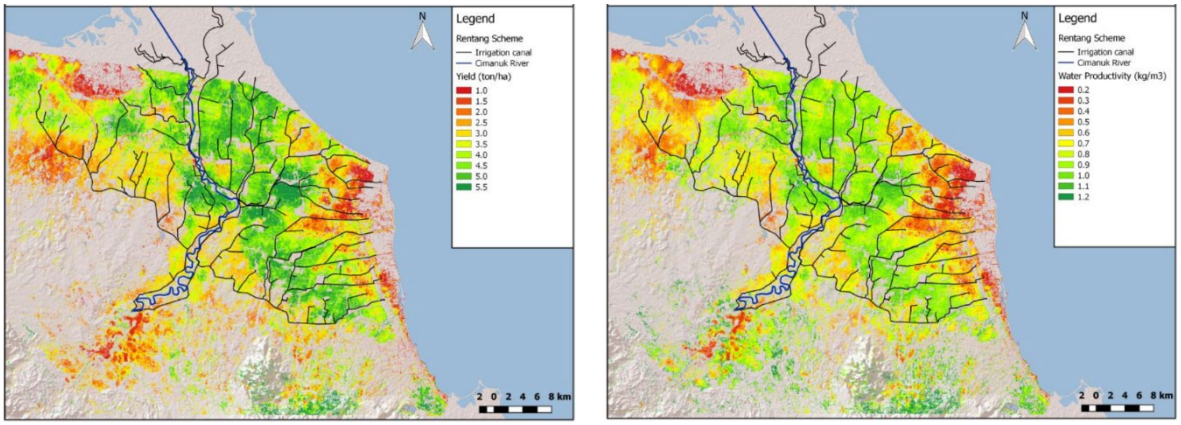

Figure 8 - (top left) Evapotranspiration (top right) ET deficit (bottom left) Yield (bottom right) WP in Rentang irrigation scheme, Java, Indonesia 15Jun – 15Oct, 2016.

52. The study area in West Java was the Rentang irrigation scheme which is a large public scheme that is dominantly under paddy rice cultivation. The ET_a in the Rentang ranges from 38 to 685 mm and the average is 473 mm with a standard deviation of 85 mm. The areas near the coast show significantly higher ET compared to the areas that are located further inland (see Figure 8).

53. The ET deficit indicates the difference between ET_a and potential ET. High ET deficit indicates water stress and can be used to identify any existing areas that suffer from the lack of availability and/or access to irrigation water. In the case of the Rentang, the ET deficit was merely 12 mm in the study season (see Figure 8) which suggests that, despite having a low WP, overall the scheme is not affected by irrigation water deficit, although pockets of higher deficit areas can be found which requires attention. The WP analysis shows that the main reason behind the low WP in the Rentang irrigation scheme is low yield observed in areas closer to the ocean, and in more upstream areas closer to the main canals maps. Yield and water productivity should both score high in an ideal situation.

54. Figure 9 shows the yield and WP of rice for every 30x30 m^2 field. The two-dimensional plot shows most of the pixels fall in a shape that is defined by a straight line at the bottom, and a curve-linear line on top. The bottom line is defined by the potential ET that is controlled by atmospheric conditions. The upper line is defined by local water management practices, including on-farm. This graph demonstrates vertical with farmers who produce the same yield but with low and high WP. This shows that a lower ET is not necessarily bad. In the verticals, farmers should move up from the bottom to the top. The horizontal show that a large group of farmers that are scoring high in WP, but their yield is low, and hence their income and perhaps even own food production. A yield of 2 ton/ha is very low, and they should target more on 3 to 6 ton/ha. In the case of the latter, assistance from agronomic extension officers is needed. Not all farms have the same potential due to soil, water, and other limitations. It is therefore often not possible to push all the farms towards the top-right corner of Figure 9.

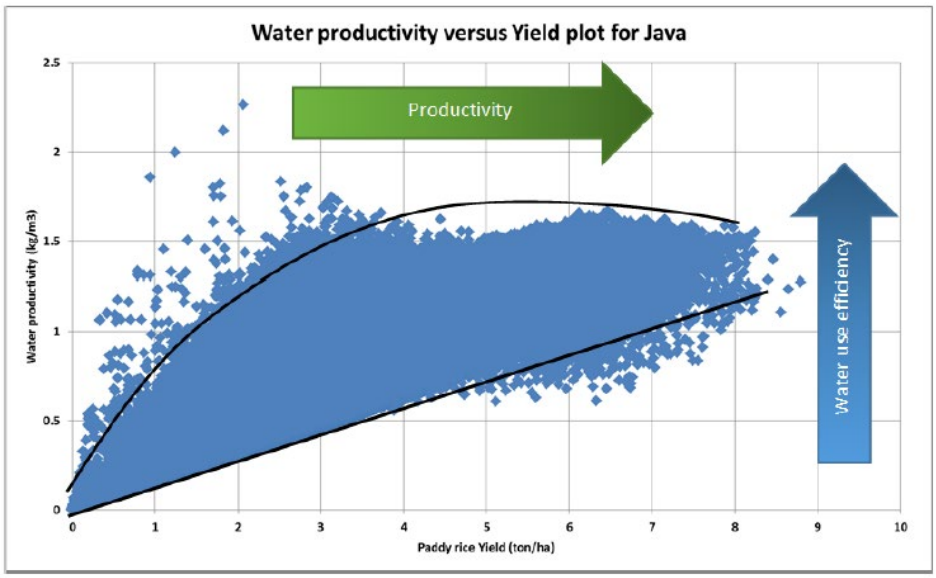

Figure 9 - The Relationship between WP and yield of rice in the Rentang scheme, 15 Jun – 15 Oct 2016.

55. A closer look reveals a correlation between proximity to saltwater bodies and regularly flooded zones and incidents of observing low yields and low WP. This analysis helps to identify priority areas for investments. Priority for interventions can be identified first even though the absolution potential is not known. Figure 10 shows two different approaches to identifying priority areas for interventions. Due to resources and/or capacity constraints, it is often not possible to allocate resources to all areas evenly in a large scheme and the decision-makers must be informed about hotspots for improvement to be able to prioritize investments. For the Rentang scheme areas shown in the figures below could be considered as focus areas for improvement.

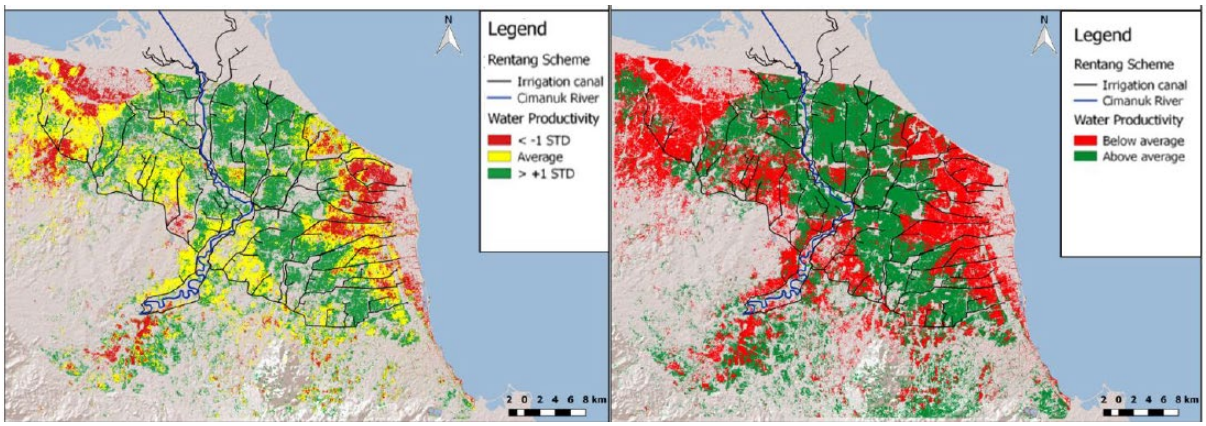

Figure 10 - Trade-offs in determining priority intervention areas. The left shows areas with WP 1 standard deviation below average, on average, and 1 SD above average. The right shows only two divisions: areas above and below average.

2. Sri Lanka

56. The aim of the pilot study was to assess the baseline condition of crop water use, yield, and water productivity in the 2016 Yala season in System H in the Mahaweli Basin. The system is located in the dry zone of Sri Lanka. It is characterized by two monsoon seasons, the drier Yala season from April to August and the wetter Maha season from September to March. The assessment was supported by the ground observations during the growing season. Satellite images from Sentinel 2, Landsat 8, Proba-V and VIIRS were combined to remove the effects of clouds and to develop time series of 30-meter resolution maps. Paddy rice is the predominant

crop in the system H. The WP analysis showed high variability in WP and points at the coexistence of poor and good irrigation management practices in the system.

57. The average WP of paddy rice was 1.15 kg/m^3 for the 2016 Yala season, similar to that of the world-wide average value for WP at 1.1 kg/m^3. The average rice yield was 5.1 ton/ha and the average ET_a was 452 mm. The spatially distributed maps of ET_a, ET deficit and yield also show high variability (see Figure 11). The coefficient of variation (CV) of WP, ET_a, and yields is 27%, 31%, and 17% respectively. The variability is higher than in other studies in Indonesia, Viet Nam, and India, indicating greater heterogeneity and at the same time higher potential for improvement by focusing on hot spots. The average ET deficit is 156 mm for the entire growing season, which translates to a 26% shortage should the demand be fully met. Water scarcity is therefore identified as the main constraint for food production in the system.

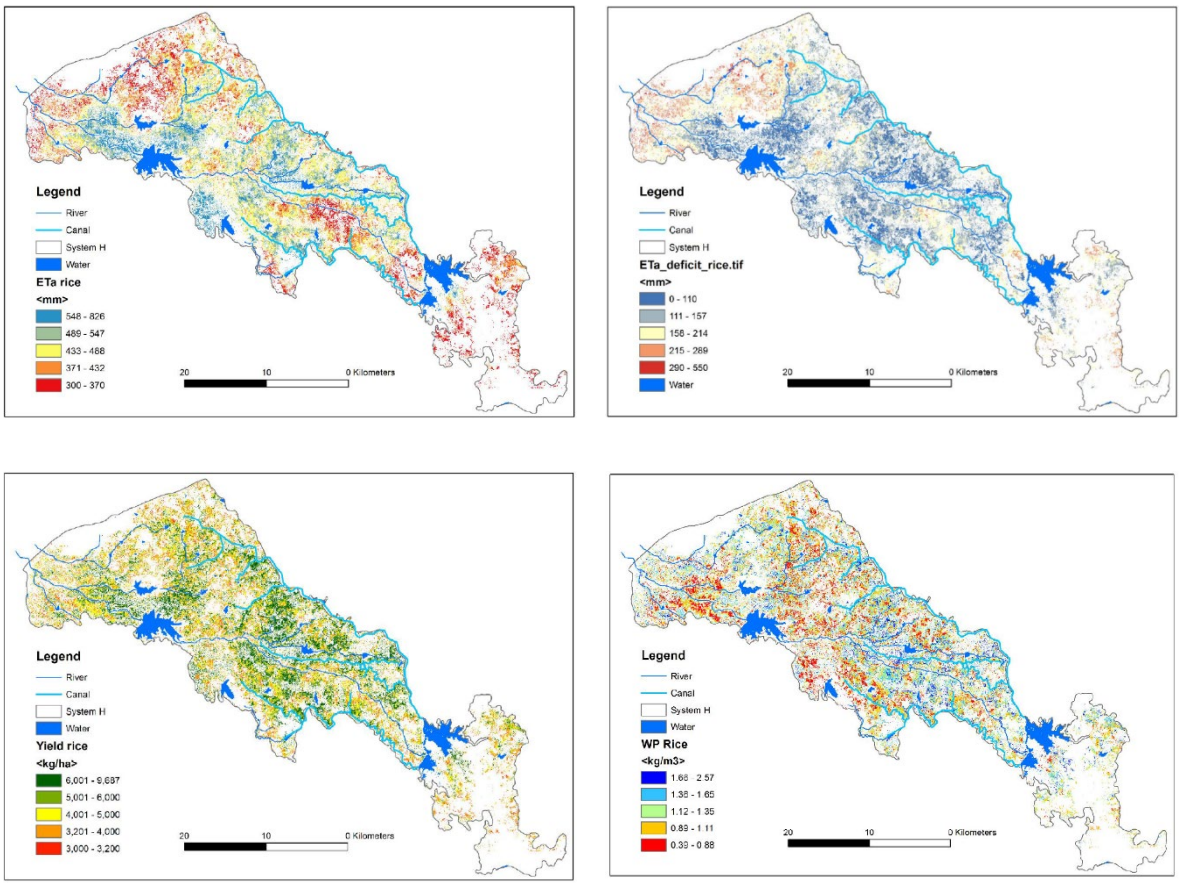

Figure 11 - (a) ET_a of rice (b) ET_a deficit (c) Rice Yield (d) Rice WP for System H in the Mahaweli Basin for the 2016 Yala season.

58. Proximity to canals, rivers, and tanks are found to be closely linked with the performance of the system. The closer a field to a canal, the more likely it will have higher yield and WP. A similar trend is observed with distance to rivers. The farms within 250-meter distance to rivers seem to have a much higher yield and WP. This pattern indicates issues with the distribution of water and the performance of the irrigation service providers in terms of the equitable and adequate distribution of water among the beneficiaries in the system.

59. Areas with low WP are often where opportunities for improvement are likely to present and where relatively bigger gains can be made with lower investments as opposed to other areas. These areas in system H are typically found in downstream areas but also spread within high performing areas. Priority for interventions can be identified first even though the absolute potential is not known. Figure 12 shows two different approaches to identifying priority areas for interventions.

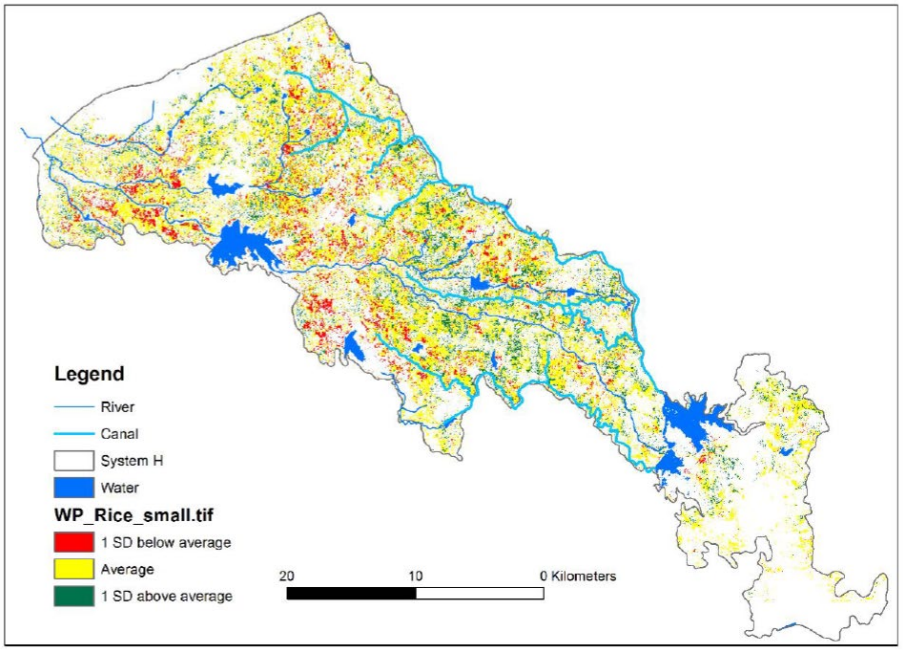

Figure 12 - Trade-offs in determining priority intervention areas in system H in the Mahaweli Basin. The areas with WP 1 standard deviation below average, on average, and 1 SD above average.

III. Water Accounting

A. Water Resources Management Challenge

60. The global freshwater demand for agriculture is expected to increase drastically over the course of the century. With the world population expected to grow from 7.3 billion in 2015 to 11.2 billion people at the end of the century and with increasing wealth, a change in diet from cereals to meat and vegetables will increase the water required to produce sufficient food (UN, 2015; Tilman and Clark, 2014). Additionally, climate change is expected to drive the increase in evaporation of agroecosystems around the world (Wada et al., 2013).

61. At the same time, increasing competition over water will affect the supply of water for agriculture. Other water use sectors, like energy production, industries and the environment are putting more pressure on water resources (Schewe et al., 2013). Currently, many regions around the world already face water scarcity, meaning there is a deficit in the water supply to meet the demand (Hoekstra et al., 2012). As demands increase and supplies decrease or stay the same, water scarcity will be increased and competition for water will intensify.

62. There is, therefore, a need to describe water resources, using clear terminology and a standard data collection system with known quality standards. Vaporization of water from land into the atmosphere – as well as water incorporated in products – produces agroecological–economical services. These services should be understood and improved if we want to maintain current per capita water availabilities and water footprints. Water Accounting can, therefore, be used as the basis for evidence based decision making and establishing agreements with riparian partners, including those across international borders.

B. What is Water Accounting?

63. Water Accounting can be defined as the systematic acquisition, analysis and communication of data and information relating to stocks and fluxes of water in natural, disturbed or heavily engineered environments, within a geographical domain such as an irrigation system, river basin or country (FAO, 2012; Batchelor et al., 2016).

64. The process of water accounting consists of several steps that need to be executed in a systematic way:

- Data on water stocks and fluxes need to be acquired. It is important to acquire data from a wide range of sources, to be able to assess the level of uncertainty of the measurements and to identify possible errors and data gaps. This assessment of the data is also important to make sure that in the end, the different stakeholders trust the data presented in the water accounts and feel confident in using the results for monitoring and planning;

- The acquired data needs to be analysed and turned into information. In order to do so, data needs to be organised in a standardised manner, for example summarised at basin or sub-basin scale. Although water accounting strives to be unbiased, there are always

choices to be made, however small, which influence the outcome. Documentation and transparency are thus important here;

- The created information needs to be processed in such a manner to clearly communicate the outcomes to stakeholders (e.g. plotting information in a diagram or graph). By doing so the information becomes more accessible and understandable to all stakeholder including non-experts.

65. By systematically acquiring, analysing and communicating information related to water resources, water accounting can thus:

- Assist in developing a common understanding of the state of water resources of a domain (such as a river basin), opposed to each stakeholder working with its own, often leading to a different understanding of a situation;
- Help to identify water related problems (such as water scarcity) and possible solutions;
- Evaluate anecdotal evidence, such as expert opinion or folklore. Water accounting can provide less biased information to check whether or not anecdotes still hold merit and thus challenge factual errors and biased views.

C. WA+: Water Accounting using remote sensing

66. Water Accounting over the years has evolved since the first introduction by Molden (1997). It started with analysing irrigation systems using observed data. Later on remote sensing information was used to provide spatially aggregated information on the performance of the irrigation systems (Bastiaanssen et al., 2000). In 2013, the Water Accounting Plus (WA+) framework was developed to analyse water accounts at river basin level (Karimi et al. 2013). WA+ integrates hydrological processes, with land use, managed water flows and the services that result from water consumption in river basins. Its objective is to achieve equitable and transparent water governance for all users and a sustainable water balance. It is mainly based on open-access earth observation data which offers several benefits:

- All data is spatial and can thus be presented on maps or can be aggregated based on other spatial data, such as land-use classes.
- No-one “owns” the water accounts, meaning they can be shared by anyone to anyone, giving all stakeholders the same (amount of) information.
- Biases in the data are consistent among different WA+ studies, allowing for comparisons between different study areas.

67. The satellite data can be complemented by hydro-meteorological datasets measured *in-situ* when available. The most important datasets used are discussed in Section 1. The results of the analyses of the data is presented through a number of fact sheets and supporting spatial maps, which are discussed in Section 2, 3 and 4.

1. Data requirements

68. In order to produce water accounts using the WA+ framework, a range of different remote sensing products is used (Table 2). Among these products, Precipitation and Actual Evapotranspiration are the most important, since they are respectively the largest source and sink

of water in a basin, i.e. they have a big influence on the water balance in a basin (see Section 2 for more on the water balance).

Table 2 - An overview of the most important type of datasets used in the WA+ framework.

Variable	Parameter	Description
Precipitation	P	Precipitation consists among others of rain and snow.
Actual Evapotranspiration	ET_a	Actual Evapotranspiration is a combination of different upward water fluxes, i.e. soil and water evaporation and transpiration.
Land-use / land-cover	LULC	A land-cover map indicates the physical land type (such as forest or agriculture), whereas land use maps show how the land is being used, e.g. agriculture can be split into rainfed or irrigated agriculture.
Leaf Area Index	LAI	Leaf-Area-Index gives an indication of the amount of foliage present in an area. A low value indicates bare soil.
Soil-Water-Index	SWI	The Soil-Water-Index is a measurement of the wetness of the soil.
Saturated Water Content	θsat	The saturated water content is a soil property that describes the maximum amount of water that can be held by the soil.
Runoff-ratio	r	The Runoff-ratio is a soil property giving the distribution between runoff and infiltration, i.e. how much precipitation infiltrates into the soil moisture and how much runs off towards surface water.
Storage Change	ΔS/Δt	The change in the total water storage in a basin is the sum of the change of storage in ground-water, surface-water and soil-moisture.
Net primary production	NPP	The net primary production indicates the mass of carbon that has been created by a plant for growing purposes.

69. WA+ is an accounting framework based on the landscape, land use is therefore an important input into the analyses. Four main categories of land and water uses are distinguished in WA+ (Karimi et al., 2013):

- Protected Land Use (PLU); areas that have a special nature status and are protected by National Governments or Internationals NGO's
- Utilized Land Use (ULU); areas that have a light utilization with a minimum anthropogenic influence. The water flow is essentially natural
- Modified Land Use (MLU); areas where the land use has been modified. Water is not diverted but land use affects all unsaturated zone physical process such as infiltration, storage, percolation and water uptake by roots; this affects the vertical soil water balance
- Managed Water Use (MWU); areas where water flows are regulated by humans via irrigation canals, pumps, hydraulic structures, utilities, drainage systems, ponds etc.

70. The underlying reason for framing these four land use categories is that their management options widely differ. The land cover map forms the basis for dividing the basin landscape into the four main land use categories in addition to using various open access databases. Protected Land Use class is based on the protected area profile from the World Database on Protected Areas (UNEP-WCMC, 2019). The areas which are designated as IUCN categories I and II are reclassified as PLU. The Managed Water Use class is compiled of irrigated agriculture, built up

areas and artificial water bodies (e.g. constructed reservoirs). Reservoirs and dams were identified using the Global Reservoir and Dam Database (GRanD) (Lehner et al., 2011). The Modified Land Use class is mainly based on rainfed agricultural land cover classes. The remaining area is defined as Utilized Land Use.

2. Sheet 1: The Resource Base

71. Results of WA+ studies are presented through maps, tables and a series of WA+ Sheets. The first of these sheets is called the Resource Base Sheet (Figure 13); it provides an overview, or summary, of much of the data presented in the subsequent sheets. The Resource Base sheet shows the water balance for an entire river basin. Below, some concepts presented in this sheet are explained in more detail.

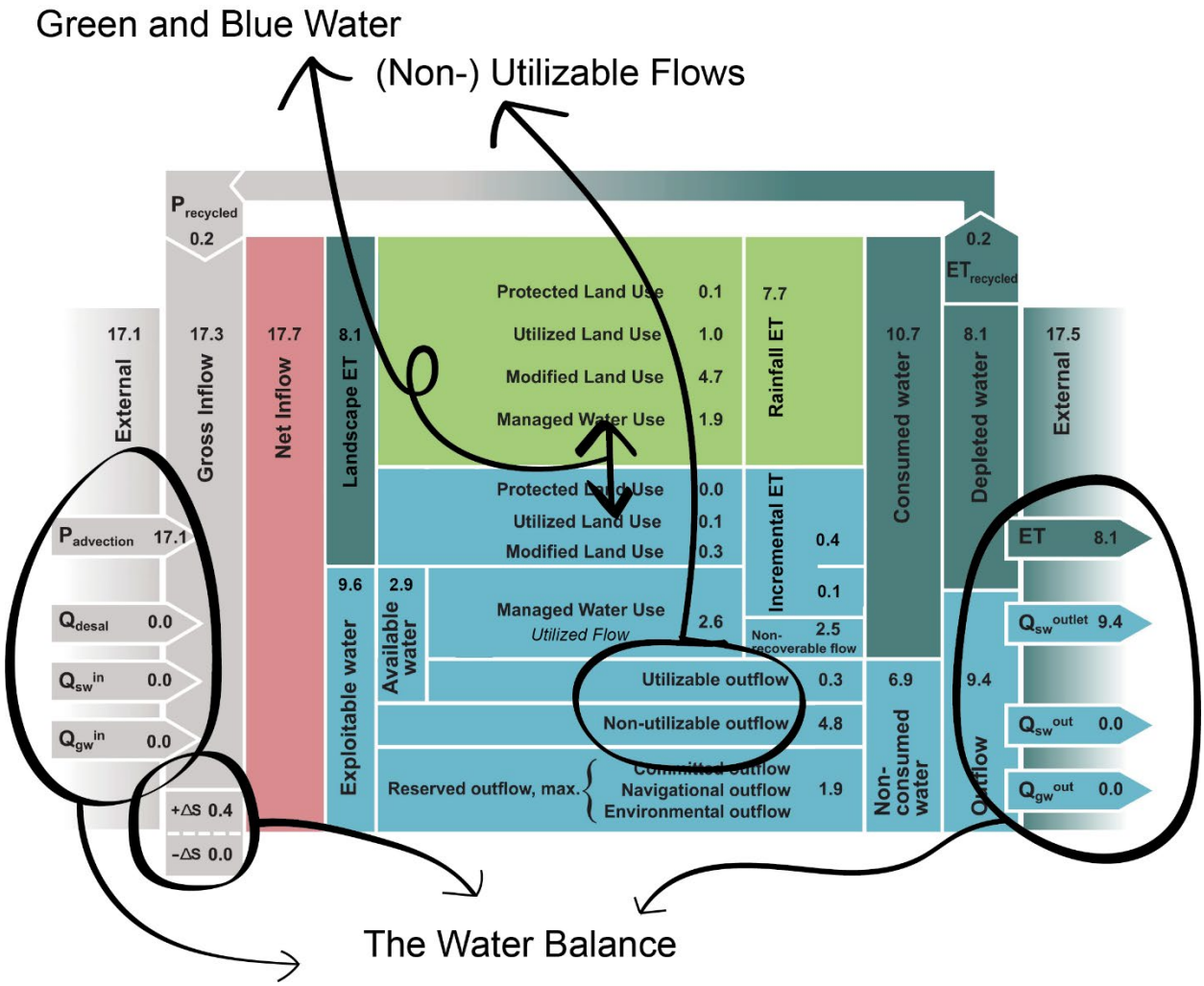

Figure 13 - WA+ Sheet 1: The Resource Base sheet: an example for the Belawan basin in Indonesia in 2013 (Michailovsky and Bastiaanssen, 2018), with an emphasis on several concepts further detailed in the following sections. All numbers in the sheet are km³/year.

a) The Water Balance

72. Just as a regular accountant evaluates the balance between revenues and expenses, an important part of the WA+ framework is the assessment of the water balance, which compares the change in storage (ΔS/Δt) through the difference between incoming (I) and outgoing (O) water flows in a certain domain over a certain period of time:

$$\frac{\Delta S}{\Delta t} = I - O \quad (10)$$

73. The evaluation of the water balance is important for several reasons. First of all, it helps water managers to understand whether a basin is facing a quantitative risk or not and helps identify drought and water scarcity situations, and monitor unsustainable practices. If, for a long enough period of time, the inflows into a basin are smaller than the outflows, sooner or later there will be a water deficit.

74. Furthermore, the water balance gives water managers an idea of the temporal variability of the availability of water resources. Depending on the temporal resolution and period of the accounts, intra- and inter-annual variability of the water resources can be established. In particular, reporting water conditions on a monthly basis allows for the identification of seasonal water shortages and excesses. It can identify periods when inflows exceed outflows, and water is stored, while during other periods, outflows can exceed the inflows and storage is depleted. Water Accounts can also identify long term trends which could indicate unsustainable utilisation of the water resources by depleting the water storage.

75. The water balance components are reflected in the Resource Base sheet of WA+. On the left side (Figure 14), the grey arrows show different water flows into the basin (adding to the *Gross Inflow*). These flows consist of precipitation (*P*, including internally recycled ET) and flows into the basin from either surface water (e.g. through inter-basin transfers) or groundwater (Q_{sw}^{in} and Q_{gw}^{in} respectively) as well as flows from desalinated water (Q_{desal}). Several remote sensing products of rainfall are available to estimate the basin precipitation, often the largest incoming flux of water in a river basin. Data on the other inflows has to be obtained from the field.

76. The grey box at the bottom left of the Resource Base sheet (ΔS), represents changes in storage within the basin. A depletion of the storage adds water to the water balance, while an increase in water storage indicates water is taken out of the water balance. The water storage depletion makes water available for the users, however, this is not sustainable in the long run. The change in storage is estimated using data obtained from the Gravity Recovery and Climate Experience (GRACE) (Luthcke et al., 2013). The *Gross Inflow* plus the change in storage becomes the *Net Inflow*.

77. The other side of the sheet shows blue arrows representing flows leaving the basin through the *Outflow*, which consists of surface water outflow (Q_{sw}^{outlet}), inter basin transfers (Q_{sw}^{out}) and through groundwater flows (Q_{gw}). The green arrow indicates the Depleted Water through evapotranspiration. Evapotranspiration (ET) is usually the largest of these flows, and can be estimated using remote sensing information. To estimate the other components of the outflow, information from field observations is required.

b) Blue and Green Evapotranspiration

78. In the WA+ framework a distinction is made between two types of evapotranspiration. Evaporated water originating directly from precipitation is termed green evapotranspiration (ET_g), while evaporated water coming from groundwater aquifers, lakes or streams is called blue evapotranspiration (ET_b). Water flowing in rivers and water stored in surface and groundwater reservoirs is defined as blue water.

79. Water in the root-zone on the other hand can consist of both green and blue water. This is either replenished through precipitation and therefore defined as green water, or water is replenished through human actions (e.g. irrigation) or through flooding, which then is defined as blue water.

80. *Landscape ET* is defined as all the ET_g and ET_b excluding water managed land use classes. The remainder of the *Net Inflow* becomes *Exploitable Water*. This is defined in this way as there is a clear distinction in how the different water flows can be managed. *Landscape ET* is strongly influenced by land-use management. Different land-use practices can influence the way precipitation is partitioned into infiltration and surface runoff, affecting the overall catchment water balance.

81. On the other hand, *Exploitable Water* is defined as the blue water resources (water in rivers, dams and groundwater) including ET_b for water managed land use class. This water is available for use and can be managed through for example diverting water for irrigation or through the construction of dams. Water allocation decisions are common management practices for managing *Exploitable Water* and it directly affects the blue water stocks and fluxes.

82. Estimating ET_g and ET_b can thus give an indication of amount of *Exploitable Water* and give an indication on the types of interventions which can support sustainable management of the basin.

83. ET_g and ET_b can be estimated through establishing a water balance for the soil moisture:

$$\frac{\Delta S_m}{\Delta t} = P - ET_a - Q_{sro} - R \tag{11}$$

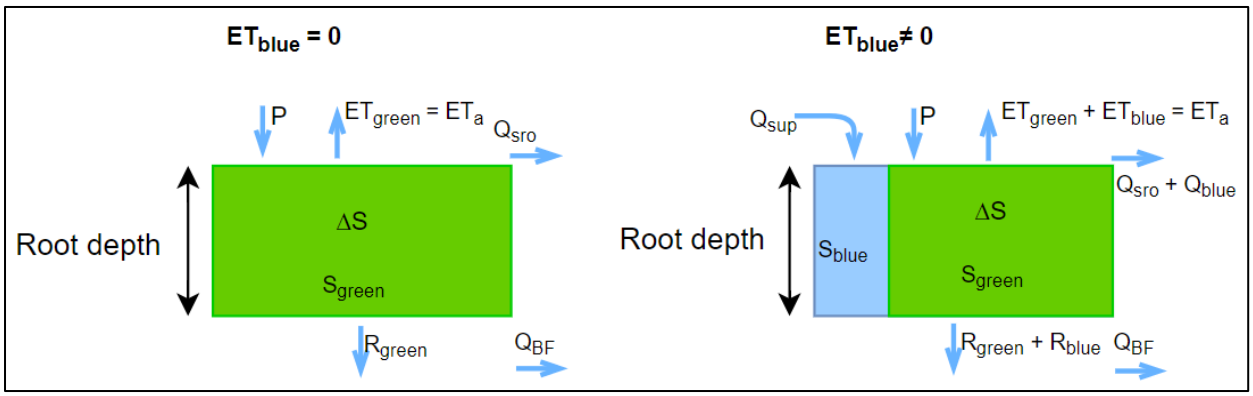

Figure 14 – The green and blue soil water balance (after FAO and IHE Delft, 2019).

84. The main input into the soil water balance is ET_a from remote sensing. When rainfall and soil moisture are sufficient to supply ET_a, ET_a becomes ET_g (ET_{green} on the left side of Figure 14). When rainfall and soil moisture are insufficient to supply ET_a, the difference becomes ET_b (ET_{blue} on the right side of Figure 14). The change in storage can either be estimated through using ASCAT soil water index from remote sensing (e.g. Wagner et al., 2013) or through tracking soil moisture storage throughout the period of assessment (e.g. FAO and IHE Delft , 2019).

c) Utilizable and non-utilizable flows

85. Besides showing the water balance and the quantities of green and blue water flows in a river basin, the Resource Base sheet also gives a breakdown of the *Exploitable Water* based on its current utilisation, estimated non-utilizable and reserved flow.The *Available Water* for further productive and economic use excludes *non-utilizable flows* and *reserved flows*.

86. *Non-Utilizable flows* are defined as the amount of water which is not available for water resources development. This results from spatial and temporal availability of the water. Part of the flow that occurs rapidly (e.g. flash floods) or precipitation that falls in the most downstream part of the basin, which often has limited options for storing water and is therefore termed non-utilizable.

87. Besides the non-utilizable flows, a portion of the blue water is reserved. This includes water which is part of a sharing agreement with a downstream country, or a portion of the water in a lake or river that needs to be left to ensure the health of the local ecosystem.

88. In most basins, part of the available water is already used (*Utilised Flow*), this includes the amount of ET_b for managed water use and *non-recoverable flow* which is a function of the pollution rate in the basin, estimated using the Grey Water footprint (Mekonnen and Hoekstra, 2015). The remainder is called *Utilizable water*, which provides an estimate on the potential for water resources development.

3. The other WA+ Sheets

89. The Resource Base sheet gives an overview of what is presented in more detail in the remaining sheets. These sheets provide in more detail specific elements, as indicated in Table 3 below.

Table 3 - An overview of the functions of the remaining WA+ sheets.

Sheet 2 : Evapotranspiration
● Quantifies water consumption for all land use classes throughout the basin. ● Describes the anthropogenic impact on ET. ● Helps to understand impact of land use planning on consumptive use. ● Relates water consumption to intended processes, by estimating (non-)beneficial ET.
Sheet 3 : Agricultural Services
● Quantifies the agricultural production (kg/ha) in terms of food, feed, timber and fish production on a basin scale. ○ Food production is estimated based on existing (coarse) global datasets for Net Primary Production (NPP) to calculate biomass production[1]. ○ Feed, timber and fish production are reported based on local data (if available). ● Presents the related water productivity (kg/m³) (see also equation 3).

[1] As these analyses provide a quick assessment using existing coarse global datasets, the accuracy of agricultural production and water productivity assessments are of lower accuracy than the assessments done following the approach presented in Chapter II

    - Based on the water consumption reported in sheet 2.
- Helps deciding on future rainfed and irrigated cropping systems.
- Indicates possibilities for saving water in agriculture, with an emphasis on non-beneficial water consumption and shifts from irrigated to rainfed crops and agroforestry systems.

Sheet 4 : Utilized Flows

- Provides an overview of all man-made withdrawals.
- Estimates natural withdrawals due to seasonal floods, shallow groundwater tables and groundwater dependent ecosystems such as forests.
- Describes surface-water and ground-water contribution to total withdrawals.
- Distinguishes between consumed and non-consumed water and shows the impact of non-consumptive water use on downstream users (i.e. terrestrial water recycling).
- Recognizes recoverable and non-recoverable flows.

Sheet 5 : Surface-water

- Quantifies the natural and actual river flows along a transect of tributaries.
- Determines the surface water availability and utilizable withdrawals in any location in the river basin.
- Describes storage in tributaries and main rivers for regulation purposes.
- Assist in the planning of infrastructure and water resources development.
- Helps preparing (surface-) water allocation plans, also for dry years.

Sheet 6 : Groundwater

- Helps to understand the role of groundwater in renewable water resources.
- Identifies aquifers which are used as a storage reservoir for droughts and their role as buffering mechanism.
- Helps preparing safe groundwater withdrawal plans and thus prevent declining groundwater tables.

4. Spatial and temporal analyses

90. The WA+ sheets provide a wealth of information related to water management in a systematic way. However, these sheets are not always easy to interpret and only provide a snapshot of the situation (either for a month or a year). For water managers, it is important to compare different years, analyse the spatial patterns of data presented in the sheets and to identify temporal trends. As much of the information presented in the WA+ sheets are aggregated from spatial maps. It is therefore possible to present the information in the form of maps as well as tables and graphs. Some examples of maps and graphs derived from WA+ studies are presented here to illustrate the value of presenting this information.

91. One important factor in a river basin context is to identify the sources and sinks of the water resources. This information can be estimated by subtracting ET_a from P. Positive values indicate net water generating areas whereas negative values indicate where water consumption is higher. Figure 15 shows the results of this analysis in the Litani river basin in Lebanon (FAO and IHE Delft, 2019). It shows that the surplus of the rainfall is generated in the highlands, and part of this water is consumed in the areas with high ET (left hand side) and negative $P\text{-}ET_a$ (right hand side) which are located in the Bekaa valley where irrigation is being practiced. Lake Quaroum is also identified as a water consuming area.

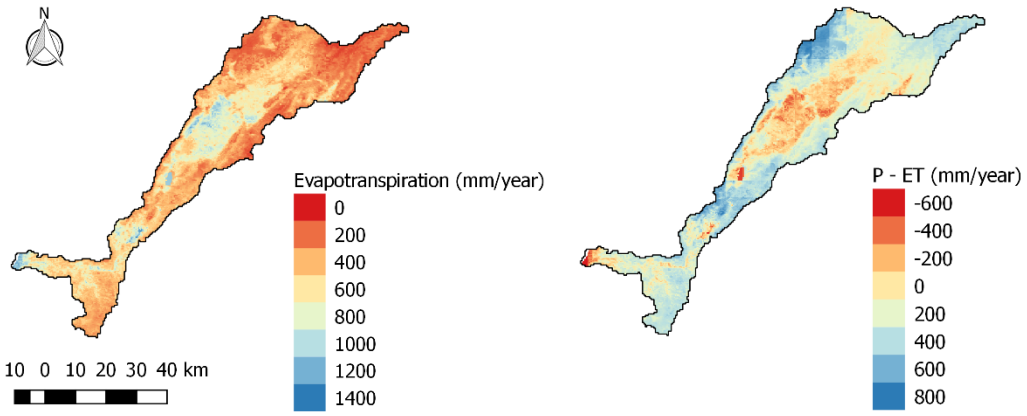

Figure 15 - The average ET_a and the average difference P-ET_a of the period 2010-2016 in the Litani basin (FAO and IHE Delft, 2019)

92. Additional information can be obtained by presenting information from individual sheets in graphs of time series. Figure 16 shows such a graph which presents the seasonal contributions of green and blue water toward total ET for Cambodia, which has a monsoon climate. During the monsoon months most of the ET is provided by rainfall (ET_g), whereas during the dry months ET reduces and the majority of the ET is provided by blue water (ET_b).

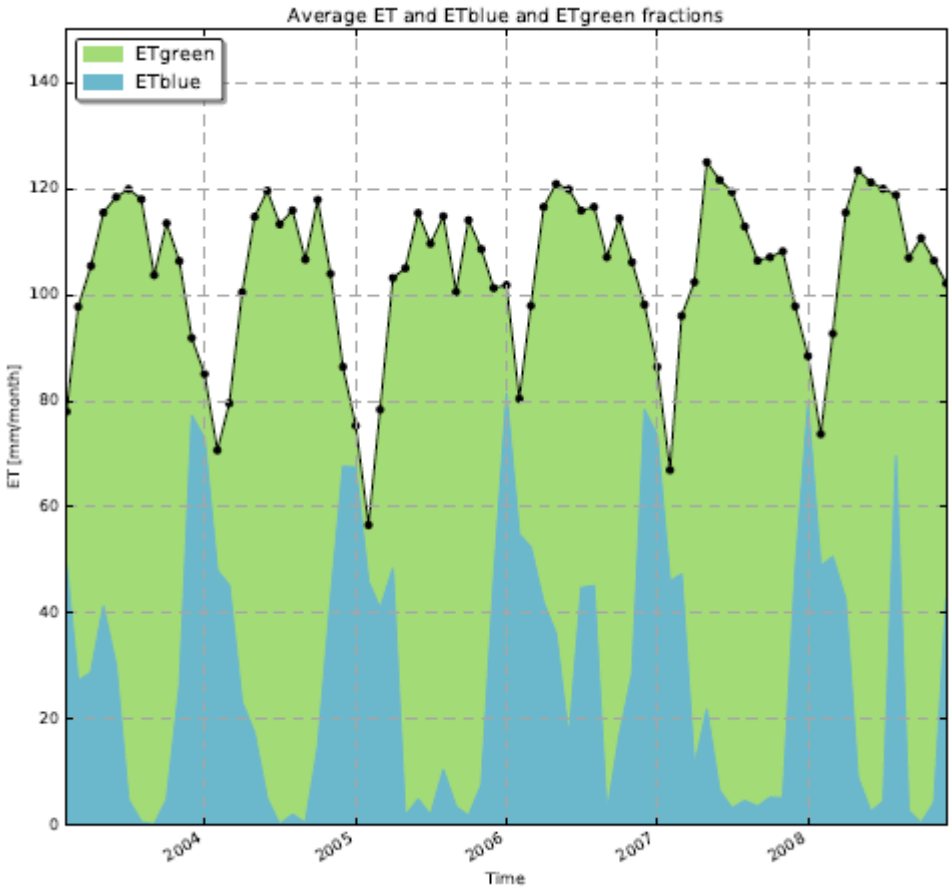

Figure 16 - Average monthly ET for the Tonle Sap basin, Cambodia, including the ET green and blue fractions (Salvadore and Bastiaanssen, 2017).

D. Case studies

93. Several studies on Water Accounting were developed in Asia as a response on the request of the ADB to conduct country water assessments as a means to plan for improved national water security (ADB, 2012). The main objective of the studies was to define sustainable water management strategies and provide inputs into the Asia Water Development Outlook. Water Accounting therefore contributes to quantifying how much water is available and who is using this water in a river basin. With expected increase in demand, solely focussing on supply management is no longer the solution, additional focus should be put towards improving productive use. Water accounting can contribute to identifying possible investment strategies which improves the overall water productivity in a river basin while maintaining the environment. Water Accounting is one of the three types of knowledge studies undertaken to pilot new approaches, tailor approaches for specific situations, and provide capacity building support to strengthen water security (ADB, 2016).

94. Even though the ultimate aim of the country water assessments is to forecast water demand vs available water resource, the current studies focussed on evaluating the past and current situation. Therefore, in 2017 and 2018, Water Accounting Plus was implemented in five countries in Asia, namely, Cambodia, India, Indonesia, Sri Lanka and Viet Nam (Figure 17). The studies were done at country level (Cambodia and Viet Nam), at state level (India) and at river basin level (Indonesia and Sri Lanka).

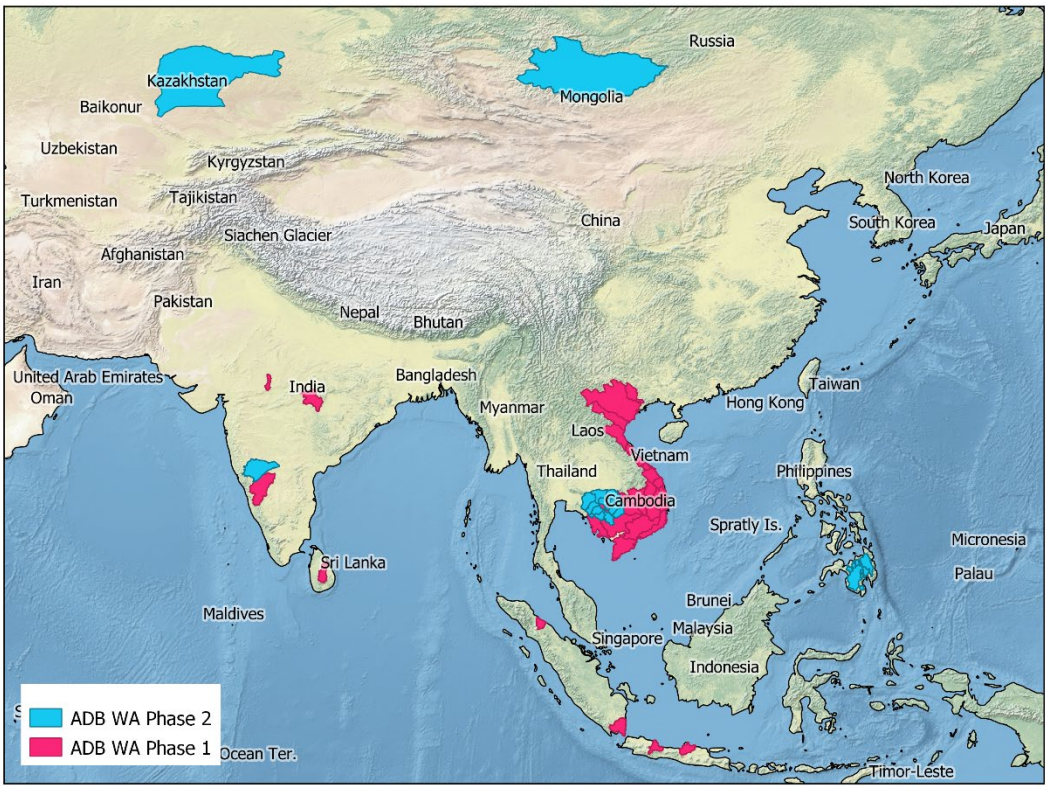

Figure 17 – Locations of the river basins for which water accounts using the WA+ framework have been created under the first and second phase of the ADB funding for water accounting studies. All of these Water accounts can be found through the following link https://wateraccounting.org/projects.html

95. Even though the overall objective of the studies was the same, the emphasis in each country was different as a response to local needs. In Cambodia and Viet Nam, country level

water resources assessments were done for the main hydrological basins and comparative assessments were performed, however no specific issue was targeted (Coerver, 2018; Salvadore and Bastiaanssen, 2017).

96. In Sri Lanka, the WA+ studies contributed towards the formulation of the proposed Mahaweli Water Security Investment Program (MWSIP) (Michailovsky and Bastiaanssen, 2018a). The aim of the MWSIP is to "invest mainly in water infrastructure and institutional capacity to improve water use efficiency and productivity for irrigated agriculture as well as providing bulk drinking water supplies from the water-rich wet zone to the water-scarce dry zone"[2]. The Water Accounting results showed that the Mahaweli river basin has sufficient utilizable outflows to allow for inter-basin transfers into the dry zone. In particular if the excess water generated during the wet season could be stored and diverted. Without additional storage, there is insufficient water to divert during the dry season (Michailovsky and Bastiaanssen, 2018a).

97. More information is provided on two case studies from Indonesia and India.

1. Belawan and Cimanuk, Indonesia

98. The WA+ studies in Indonesia focussed on supporting the formulation of the proposed Enhanced Water Security Investment Program (EWSIP) for four river basins on Java and Sumatra islands. The EWSIP aims to meet rising demands for irrigation and non-agricultural use and minimize spatial and temporal variations in water availability by improving water storage and conveyance[3].

99. The results of two of these case studies are presented here, the Belawan basin on the island of Sumatra and Cimanuk on the island of Java. The Cimanuk basin with an area of 7,692 km^2 is characterized by high variability of seasonal water availability and while Belawan basin with an area of 6,046 km^2 has low seasonal variability. Annual rainfall in an average year in the basins are 2,685 and 3,000 mm/year, whereas actual evapotranspiration is 1,268 and 1,334 mm/year for Belawan and Cimanuk respectively (Figure 18).

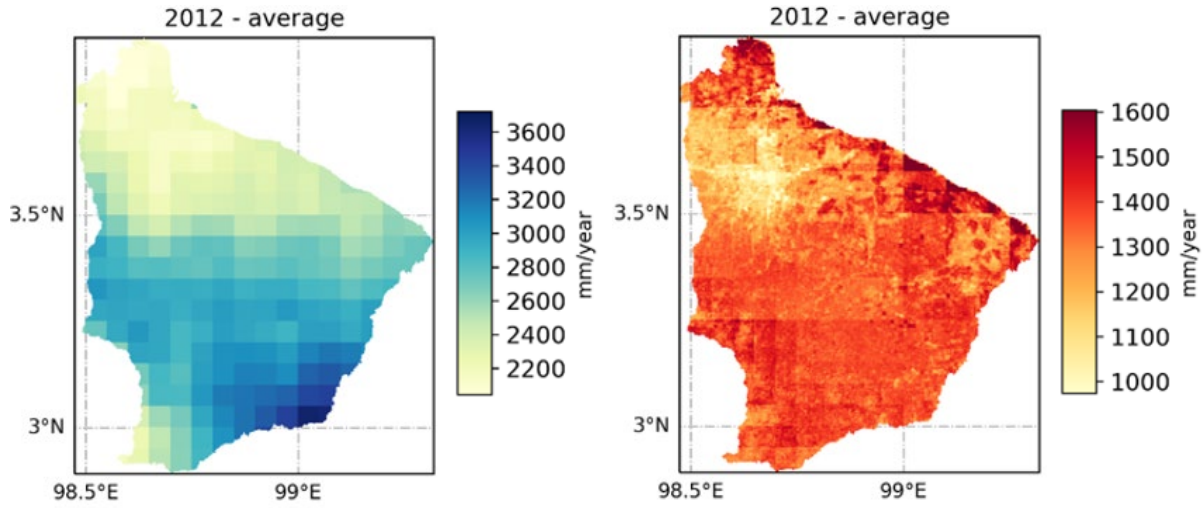

[2] http://mwsip.lk/index.php?option=com_content&view=article&id=6&Itemid=131&lang=en
[3] https://www.adb.org/projects/51157-001/main#project-pds

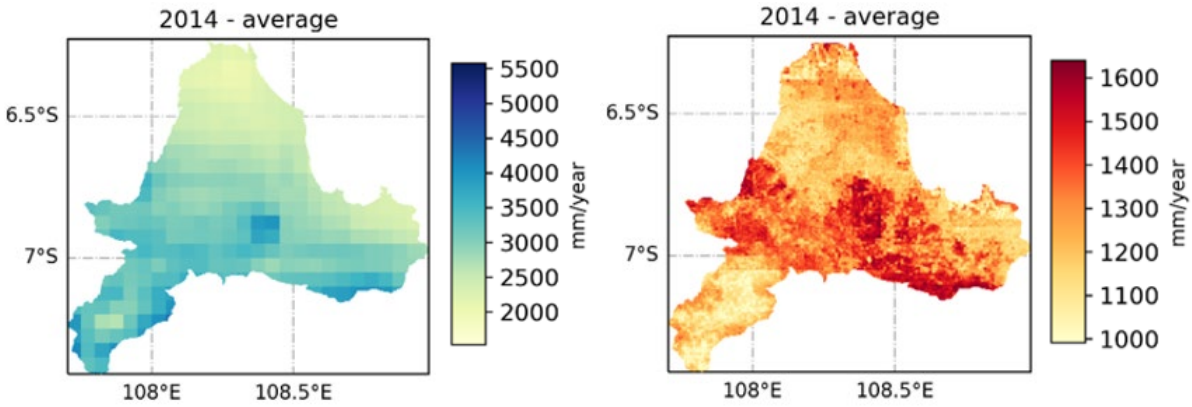

Figure 18 – Precipitation and Evapotranspiration in an average year for Belawan and Cimanuk basin, Indonesia (Michailovsky and Bastiaanssen, 2018b).

100. The Cimanuk basin has 18 different land uses types based on the WA+ land use classification and the majority of the area, about 83%, is covered by rainfed and irrigated crops (Figure 18). The major land use type in the Cimanuk basin is wet-rice field (Sawah) of which an estimated 59% is irrigated and 41% rainfed. The total rainfed area in the basin is 3,145 km^2 of which 58% is cerial crops. The total irrigated area is 3,299 km^2 of which 80% is for cereal crops. For Belawan the 78% of the total area is covered by rainfed and irrigated crops. The rainfed crop area is 3,604 km^2 of which 63% is dedicated for cereals and the total area covered by irrigated crops is 1,150 km^2 of which about 73% is for cereals.

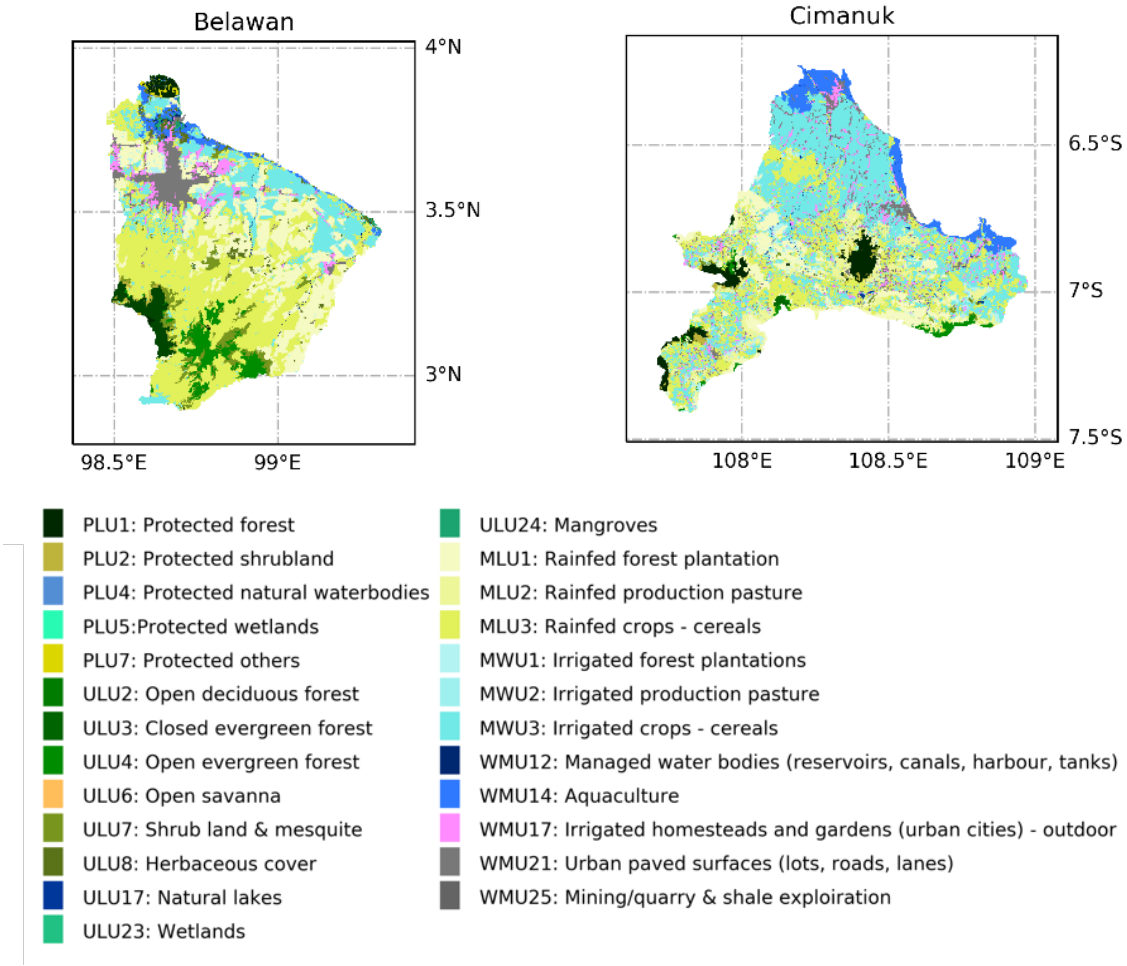

Figure 19 – WA+ land use classes in Belawan and Cimanuk basin, Indonesia (Michailovsky and Bastiaanssen, 2018b).

a) WA+ sheet 1 The Resource base

101. At basin level, determination of the main water balance components provides information about the possibility for further water resources development. The water resources situation of the basins were assessed and the results are presented in Figure 20. On a yearly basis, both basins were found to have surplus water (positive P-ET) indicating sufficient water resources for further development (Figure 20).

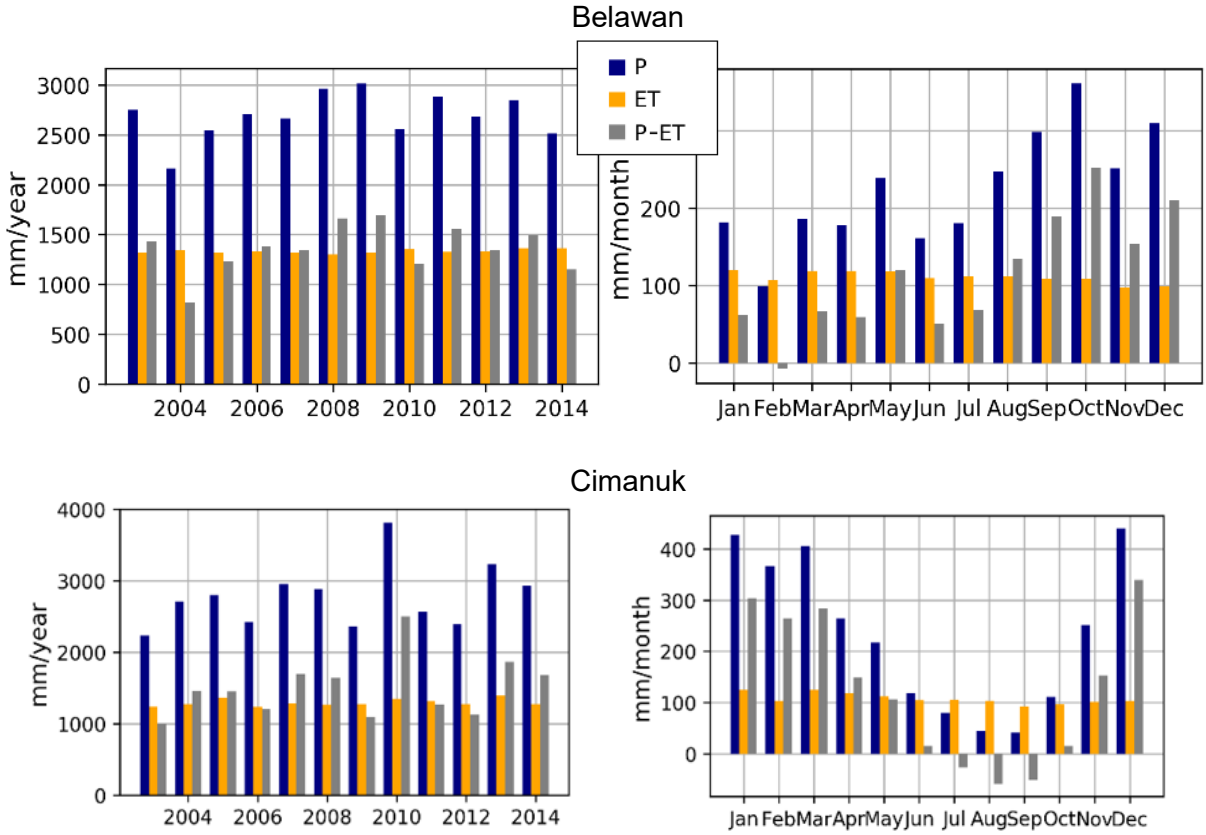

Figure 20 - Graphs showing the yearly total (left) and monthly average (right) precipitation, actual evapotranspiration and their difference for the Belawan and Cimanuk basin, Indonesia (Michailovsky and Bastiaanssen, 2018b).

102. The net water generation however is seasonal, following the pattern of the monsoon (see right side of Figure 20). For the Belawan basin, monthly precipitation is greater than the monthly evapotranspiration (positive P-ET) depicting no seasonal water shortage, whereas for Cimanuk (as well as the two other basins) a water deficit occurs during the dry season (especially July to September).

103. Figure 21 shows the different components of the total outflow of the two basins. *Non-Recoverable* refers to water which is polluted and cannot be used without appropriate treatment. *Non Utilizable* flow is from flash floods and runoff generation in the lowlands and *Committed* is to satisfy the environment flow requirements. In the Belawan basin, even though the river flows througout the year, a large part is polluted (*Non-Recoverable*). Only part of the flow is utilizable. One the other hand, the utilizable flows in the Cimanuk basin are much higher and consistent. However in all cases, utilizable flows are reduced to zero during the dry season.

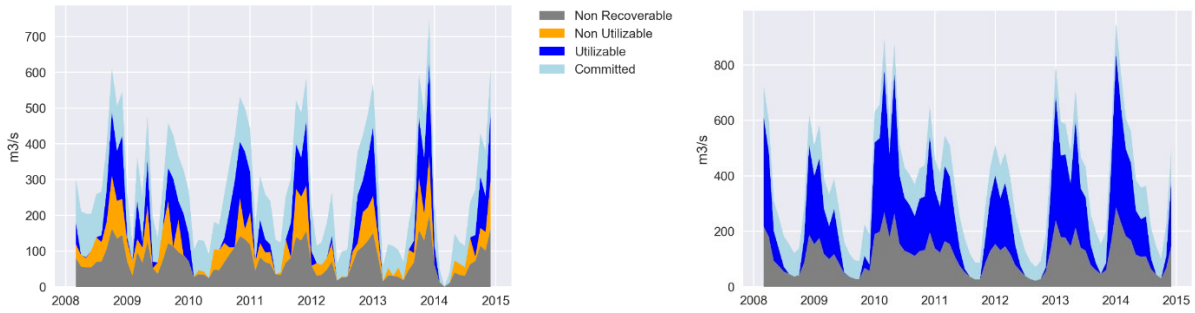

Figure 21- Total outflow of the Belawan (left) and Cimanuk (right) basins separated into Non-recoverable, non-utilizable, Utilizable and committed flows (Michailovsky and Bastiaanssen, 2018b).

104. The long term change in storage as observed by GRACE and calculated using the WA+ framework in the two basins does not show significant trends (Michailovsky and Bastiaanssen, 2018). Only the GRACE data for Belawan shows an increasing trend in water storage, although these are not consistent with the values calculated using the WA+ framework (Figure 22). The general observation is that there is no issue of overexploitation of water resources in the basins under current conditions.

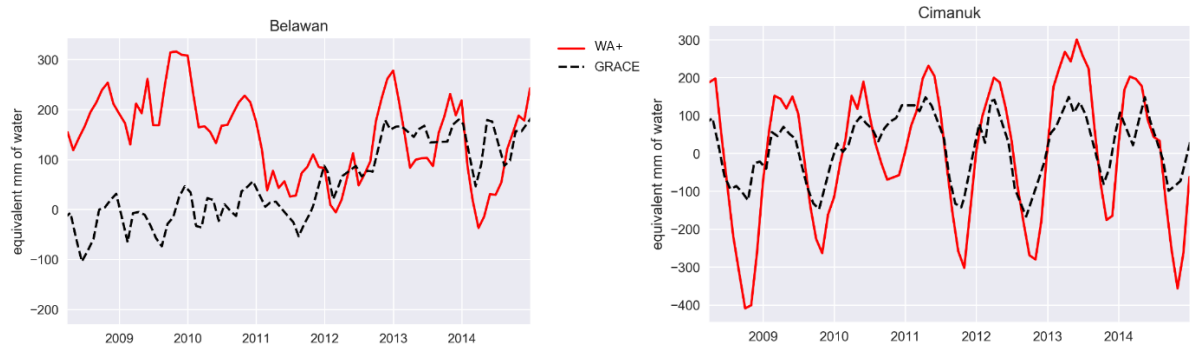

Figure 22 – Water Storage in equivalent mm of water as calculated from WA+ and GRACE for the Belawan (left) and Cimanuk (right) basins (Michailovsky and Bastiaanssen, 2018b).

b) WA+ Sheet 3. Crop water consumption and productivity

105. The WA+ study includes estimation of the crop water consumption, i.e. the water consumed through ET over cropped areas during the growing season from both irrigated and rainfed agriculture. The average values for crop water consumption for irrigated and rainfed areas averaged accross the Cimanuk basin are summarized in Table 4.

Table 4- Crop Water Consumption, Cimanuk

	Rainfed	**Irrigated**
YEAR	*km³/season*	
2009	2.59	3.82
2010	2.65	3.95
2014	1.88	3.07

106. Irrigated rice was found to have average land productivities (total biomass production per unit of land area) of between 1,905 and 3,620 kg/ha/season for rainfed rice and between 5,245 and 7,269 kg/ha/season for irrigated rice (Table 5). Water productivity is also higher for irrigated rice, with values between 0.55 kg/m^3 and 0.73 kg/m^3 for irrigated rice vs. values between 0.53

kg/m^3 and 0.57 kg/m^3 for rainfed rice (Table 5). Only during a wet year are the water productivity values between rainfed and irrigated rice similar. These values are well below the global average of 1.1 kg/m^3 for paddy rice. There is therefore a potential for either increasing productivity using the same amount of water, or to decrease water consumption without affecting the productivity.

Table 5: Land and Water Productivity, Cimanuk

		Rainfed	Irrigated	Rainfed	Irrigated
YEAR	Crop Type	*kg/ha/season*		*kg/m^3*	
2009 (dry)	Rice	3,620	7,269	0.56	0.73
	Feed crops	7,786		1.15	
2010 (wet)	Rice	3,471	5,947	0.53	0.55
	Feed crops	7,383		1.07	
2014 (average)	Rice	1,905	5,245	0.57	0.72
	Feed crops	4,086		1.15	

107. The analyses show that agriculture is one of the largest water consumers in these basins, accounting for upto 70% of the managed water use. The analyses also show that crop water productivity is well below the global average and more emphasis should be placed on improving crop water productivity to either be able to produce more crops with the same amount of water, or to use less water while maintaining crop production.

108. The overall conclusion from the WA+ studies in the two basins in Indonesia is that there is sufficient utilisable flow during the wet season, which can be captured through carefully planning water storage systems to make water available for dry season irrigation. However, this development should be carefully considered so that social and environmental needs are met. According to Mekonnen and Hoekstra (2015), roughly 27-30% of the water resources in the Belawan and Cimanuk basins is polluted up to a level is it considered non-recoverable. Therefore, more water could also be made available if wastewater is treated or made available for re-use in irrigated agriculture.

2. India - Madhya Pradesh and Karnataka

109. In India, the WA+ studies were implemented in two states, Madhya Pradesh and Karnataka. In Karnataka the analyses were carried out for the Tungabhadra basin. For the purpose of illustrating the WA+ approach, we focus on the analyses done in Madhya Pradesh. Here the results of two river basins, the Wainganga and Kali Sindh are presented (Figure 23; Salvadore and Bastiaanssen, 2018). The Kali Sindh basin with an area of 3,771 km^2 is relatively flat and consists of large alluvial flood plains. The Wainganga basin has an area of 18,397 km^2 where the river Wainganga originates in the Mahadeo Hills and drains into the large floodplains located in the lower parts of the basin.

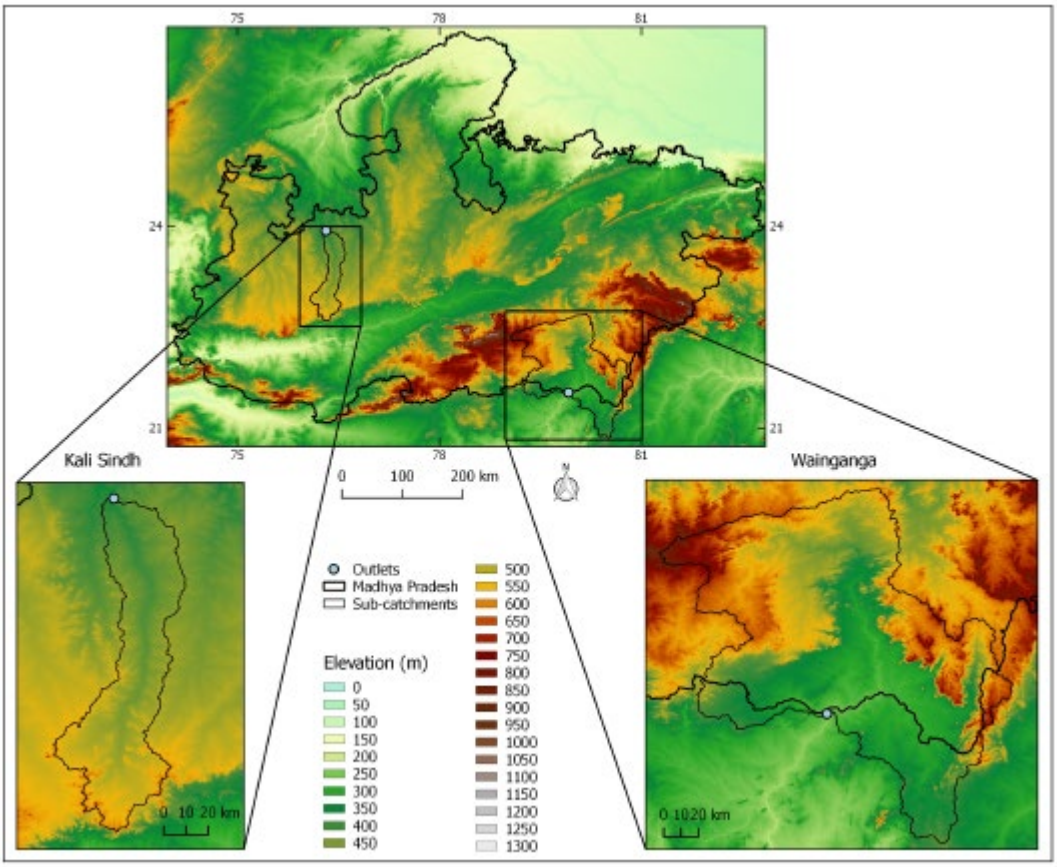

Figure 23 – Location of the Kali Sindh and Wainganga basins in Madhya Pradesh (Salvadore et al., 2018).

110. For the period considered for the water accounts (2010-2013), rainfall varies between 1,043-1,627 mm/year in the Kali Sindh basin and 1,514-1,972 mm/year for the Wainganga basin. Actual evapotranspiration varies between 609 -731 mm/year in the Kali Sindh basin and 715-989 mm/year in the Wainganga basin (Salvadore et al., 2018). Both basins are net water generators at annual scale meaning there is a surplus rainfall which is not consumed through ET, however on a monthly scale this translates to only 3 to 4 months of surplus precipitation (Figure 24).

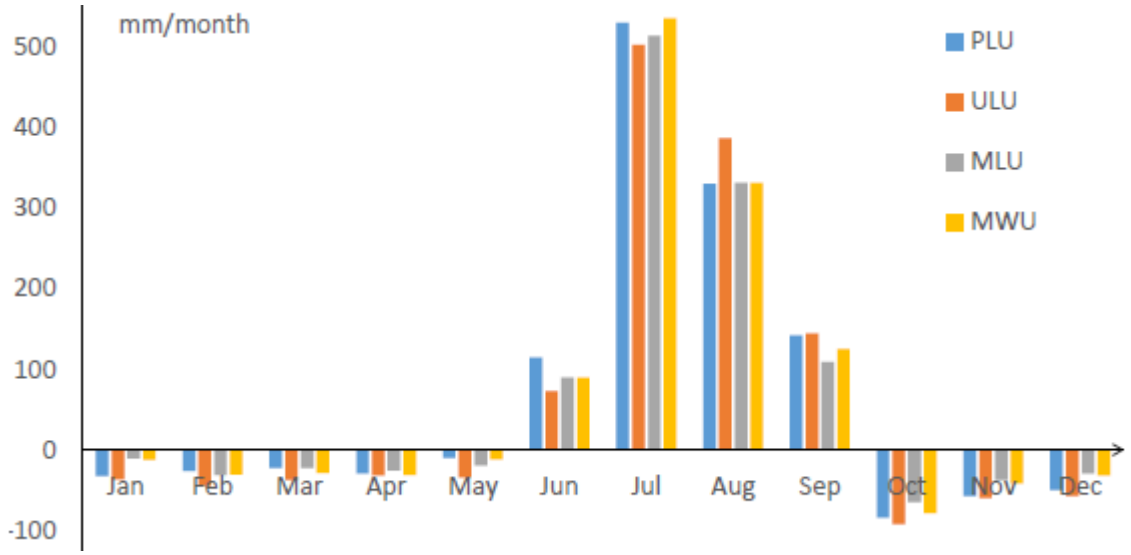

Figure 24 – Mean monthly water yield for the different WA+ land use classes in the Wainganga basins in Madhya Pradesh for 2010-2013 (Salvadore et al., 2018).

111. Agriculture is an important economic sector in Madhya Pradesh, covering large areas of both basins. In Kali Sindh, 46% of crops are rainfed and 50% irrigated while in Wainganga 34% is rainfed and 41% irrigated. The remainder of the area in Wainganga basin is covered by a large forest. Rainfed rice is the most important crop grown in the Wainganga basin, typically during the monsoon season, whereas in the Kali Sindh basin, chickpea is the main crop grown under irrigation, but is also grown under rainfed conditions (Table 6). The agricultural sector in Madhya Pradesh is aiming to increase agricultural production using the limited available water resources. Therefore discussions are ongoing to both renovate old irrigation schemes and development new ones.

a) WA+ Sheet 1 The Resource Base

112. WA+ sheet 1: the Resource Base, provides a general overview of the over-exploitation, unmanageable, manageable, exploitable, reserved, utilized and utilizable flows at river basin scale. The results of the WA+ sheet one for 2011, a typical year, for both basins is provided in Figure 25. For the Kali Sindh basin the analyses show that there is no utilizable outflow and there is insufficient water available to fulfil the minimum flow requirement (*Reserved outflow*). On the other hand, the Wainganga basin has significant utilizable flows, almost 50% of the available water can still be utilized when considering an annual time scale.

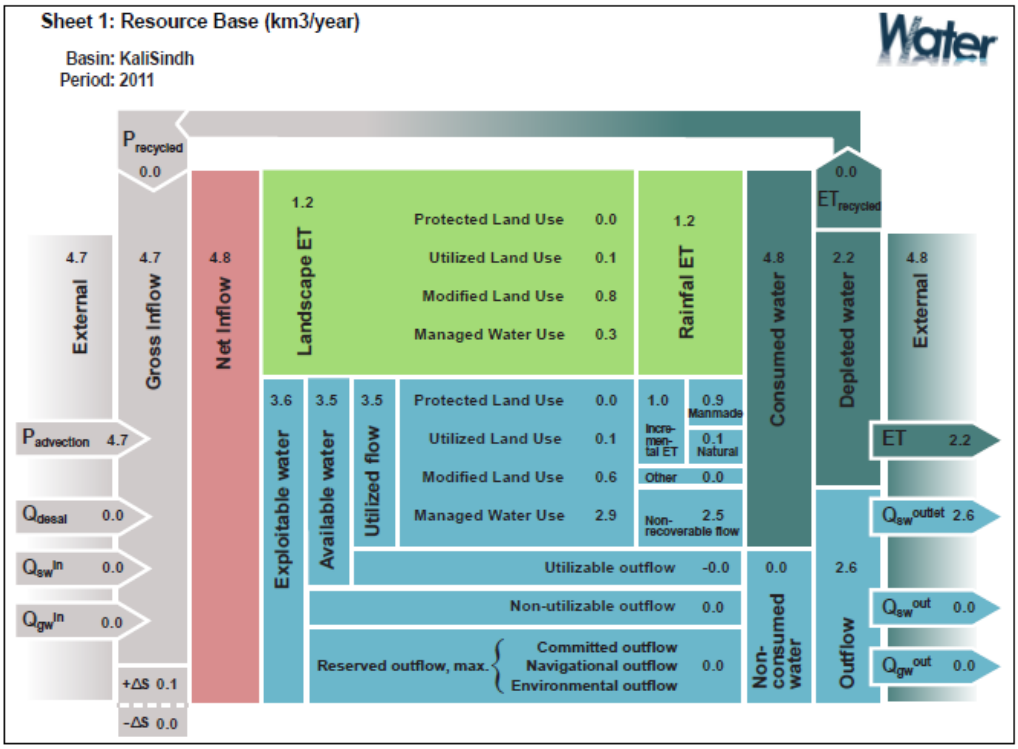

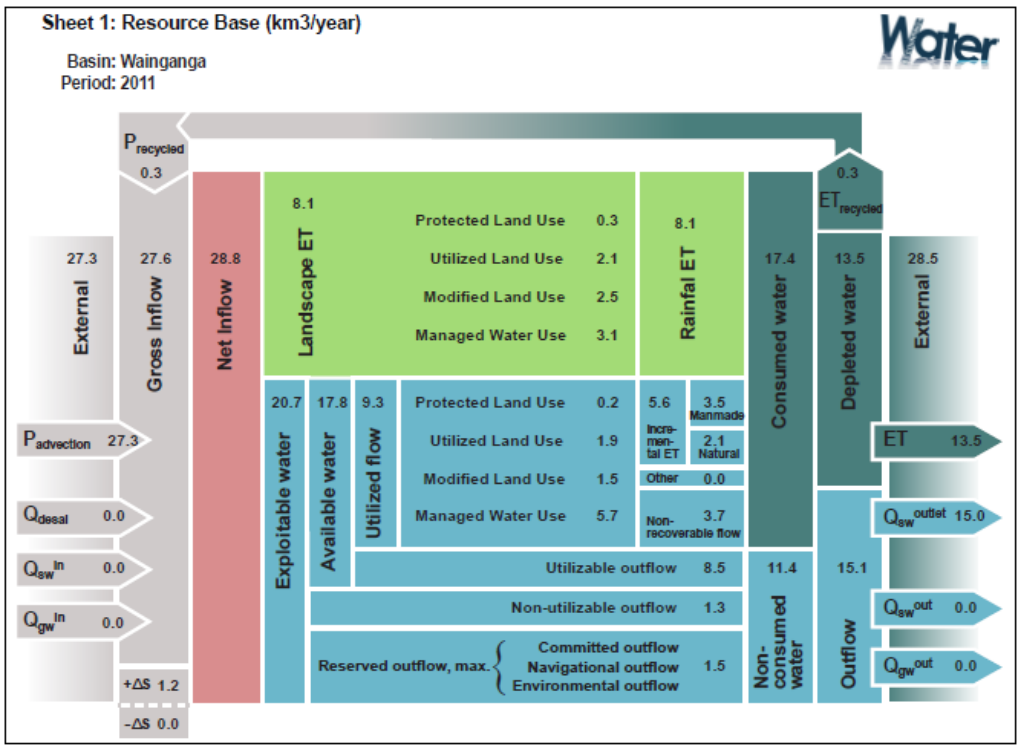

Figure 25 – Resource base sheet for the Kali Sindh and Wainganga basins in Madhya Pradesh for the year 2011 (Salvadore et al.,2018).

113. For het Wainganga basin, even though there is suffient water at annual time scale, the inter-annual variability shows a different picture (Figure 26). During the monsoon season, water accumulates in the basin and is stored, and it is depleted in the dry season. Over the period analysed (2010- 2013) an overall depletion of storage was observed. This should be monitored for longer term trends.

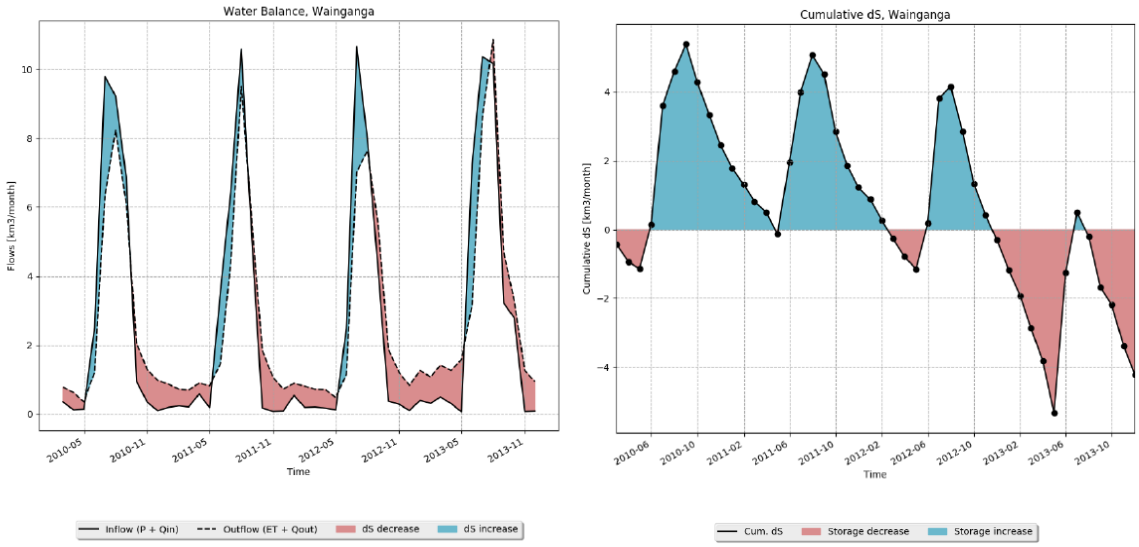

Figure 26 – Temporal variations of the main water balance components (left) and cumulative storage variation in the Wainganga basin in Madhya Pradesh for the years 2010 to 2013 (Salvadore et al., 2018).

b) WA+ Sheet 3 Crop water consumption and productivity

114. Agriculture is the main water consumer in both basins. In the Kali Sindh basin, 95% of total evapotranspiration is from agriculture, whereas in the Wainganga basin, 66% is from agriculture. WA+ sheet 3 Agricultural services is presented in Table 6. The values of land and water productivity for the cereal crops are generally low when compared to global figures, but these are in line with the production values reported for India. Irrigated areas generally have higher crop yield and water productivity than rainfed systems, particularly as they can produce two crops per year.

Table 6: Crop statistics for the year 2011 for the two basins (Salvadore et al. 2018).

WA+ crop class	Main crop type	Area [km^2]	Yield [kg/ha]	Food Prod. [Mt/season]	ET [km^3/season]	WP [kg/m^3]
Kali Sindh						
Leguminous Rainfed	Chick peas	297.3	779	0.023	0.03	0.84
Leguminous Irrigated	Chick peas	1,863.6	1,347	0.251	0.28	0.89
Fruits & Nuts Rainfed	Oranges	8.2	12,037	0.010	0.01	1.77
Oil Seeds Rainfed	Soybean	1,416.2	1,066	0.151	0.6	0.25
Wainganga						
Cereals Rainfed	Rice/ Wheat	3,827.5	1,771	0.678	0.83	0.81
Cereals Irrigated	Rice/ Wheat	7,267.3	3,187	2.32	2.18	1.06
Oil Seeds Rainfed	Soybean	2,163.3	1,228	0.266	0.51	0.52

115. The land and water productivity of both basins was found to be well below the global average for similar crops and systems. Investing in rehabilitating irrigation schemes to improve water use efficiency is therefore recommended. In the Kali Sindh basin, all water is utilized and expansion of irrigated areas is not recommended, whereas for the Wainganga basin, excess utilizable flow is available in most wet seasons, however the water storage seems to be over-exploited. Carefully planned storage systems could be considered for expanding dry season and allowing irrigation in dry years, however, a longer term and more detailed analyses would be needed to confirm this.

IV. References

Allen, R.G. (1996). Assessing Integrity of Weather Data for Reference Evapotranspiration Estimation. *Journal of Irrigation and Drainage Engineering* 122 (2): 97–106.

Allen, R.G.; Pereira, L.S.; Raes, D., Smith, M. (1998). Crop evapotranspiration – Guidelines for computing crop water requirements. FAO Irrigation and Drainage Paper, No. 56, FAO, Rome

Bastiaanssen, W.G.M. (1995). Regionalization of surface flux densi-ties and moisture indicators in composite terrain, Ph.D. thesis, Agricultural University, Wageningen, The Netherlands, p. 288.

Bastiaanssen, W.G.M., Menenti, M., Feddes, R.A., Holtslag, A.A.M. (1998). A Remote Sensing Surface Energy Balance Algorithm for Land (SEBAL). 1. Formulation. Journal of Hydrology 212, 198-212.

Bastiaanssen, W.G.M., Pelgrum, H., Wang, J., Ma, Y., Moreno, J.F., Roerink, G.J., van der Wal, T. (1998). A Remote Sensing Surface Energy Balance Algorithm for Land (SEBAL).: Part 2: Validation. Journal of Hydrology 212, 213-229.

Bastiaanssen, W.G.M., van der Wal, T., Visser, T.N.M. (1996). Diagnosis of Regional Evaporation by Remote Sensing to Support Irrigation Performance Assessment. Irrigation and Drainage Systems 10 (1): 1–23.

Bastiaanssen, W.G.M. (2000). SEBAL-based sensible and latent heat fluxes in the irrigated Gediz Basin, Turkey. Journal of Hydrology, 229(1-2), 87-100.

Bastiaanssen, W.G.M., Molden, D.J., Makin, I.W. (2000). Remote sensing for irrigated agriculture: examples from research and possible applications. Agricultural water management, 46(2), pp.137-155.

Batchelor, C., Hoogeveen, J., Faures, J.-M., Peiser, L. (2016) "Water accounting and auditing. A sourcebook." FAO Water Reports no. 43, 212 p.

Coerver, B. (2018). Water Accounting Plus in 16 Vietnamese basins. Report submitted to ADB. 16 p.

FAO (2012) "Coping with water scarcity: An action framework for agriculture and food security". FAO Water Reports No, 38, 78 p.

FAO and IHE Delft (2019). Water accounting in the Litani River Basin – Remote sensing for water productivity. Water accounting series. Rome. 56 p.

Hoekstra, A.Y., Mekonnen, M.M., Chapagain, A.K., Mathews, R.E., Richter, B.D. (2012). Global monthly water scarcity: blue water footprints versus blue water availability. PLoS One, 7(2):e32688.

Karimi, P., Bastiaanssen, W.G.M., Molden, D. (2013). Water Accounting Plus (WA+)–a water accounting procedure for complex river basins based on satellite measurements. Hydrology and Earth System Sciences, 17(7), 2459-2472.

Kustas, W.P., Blanford, J.H., Stannard, D.I., Daughtry, C.S.T., Nichols, W.D., Weltz, M.A. (1994). Local energy flux estimates for unstable conditions using variance data in semiarid rangelands. Water Resources Research 30(5), 1351-1361.

Lehner, B., Reidy Liermann, C., Revenga, C., Vorosmarty, C., Fekete, B., Crouzet, P., Doll, P., Endejan, M., Frenken, K., Magome, J., Nilsson, C., Robertson, J.C., Rodel, R., Sindorf, N., Wisser, D. (2011). Global Reservoir and Dam Database, Version 1 (GRanDv1): Reservoirs, Revision 01. Palisades, NY: NASA Socioeconomic Data and Applications Center (SEDAC).https://doi.org/10.7927/H4HH6H08. Accessed 5 August 2019.

Luthcke, S.B., Sabaka, T.J., Loomis, B.D., Arendt, A.A., McCarthy, J.J., Camp, J. (2013). Antarctica, Greenland and Gulf of Alaska land-ice evolution from an iterated GRACE global mascon solution. J. Glaciol. 59, 613–631. https://doi.org/10.3189/2013JoG12J147

Mekonnen, M.M., Hoekstra, A.Y. (2015). Global Gray Water Footprint and Water Pollution Levels Related to Anthropogenic Nitrogen Loads to Fresh Water. Environmental Science and Technology, 49(21), 12860–12868. http://doi.org/10.1021/acs.est.5b03191

Michailovsky, C., Bastiaanssen, W. (2018a). Water Accounting in Sri Lanka. The Mahaweli River basin – final report. Report submitted to ADB. 23 p.

Michailovsky, C., Bastiaanssen, W. (2018b). Water Accounting in Indonesia – Pilot studies on Java and Sumatra – final report. Report submitted to ADB. 49 p.

Molden, D., 1997. Accounting for water use and productivity. SWIM paper 1. International Water Management Institute, Colombo, Sri Lanka. 42 p.

Molden, D., Sakthivadivel, R. (1999). “Water accounting to assess use and productivity of water." International Journal of Water Resources Development 15 (1-2): 55-71.

Salvadore, E., Bastiaanssen, W. (2017). Water Accounting in selected Asian river basins: Pilot study in Cambodia. Report submitted to ADB. 58 p.

Salvadore, E., Michailovsky, C., Bastiaanssen, W. (2018). Water Accounting in selected Asian river basins: Pilot study in Madhya Pradesh (India). Report submitted to ADB. 56 p.

Salvadore, E., Michailovsky, C., Bastiaanssen, W. (2018). Water Accounting in selected Asian river basins: Pilot study in Cambodia. Report submitted to ADB. 49 p.

Santos, C.A.C., Bergson, G.B., Bernardo, B.S., Tantravahi, V.R.R. (2010). Assessment of Daily Actual Evapotranspiration with SEBAL and S-SEBI Algorithms in Cotton Crop. Revista Brasileira de Meteorologia 25 (3): 383–392.

Schewe, J., Heinke, J., Gerten, D., Haddeland, I., Arnell, N.W., Clark, D. B., Dankers, R., Eisner, S., Fekete, B.M., Colon-Gonzalez, F. J., Gosling, S.N., Kim, H., Liu, X., Masaki, Y., Portmann, F.T., Satoh, Y., Stacke, T., Tang, Q., Wada, Y., Wisser, D., Albrecht, T., Frieler, K., Piontek, F., Warszawski, L., Kabat, P. (2013). Multimodel assessment of water scarcity under climate change. Proceedings of the National Academy of Sciences, 111(9), pp.3245-3250.

Shuttleworth, W.J., Gurney, R.J., Hsu, A.Y., Ormsby, J.P. (1989). FIFE: the variation in energy partitioning at surface flux sites. Proc. Baltimore symp., IAHS publ. no. 186: 67–74.

Teixeira, A., de Castro, H., Bastiaanssen, W.G.M., Ahmad, M.D., Moura, M.S.B., Bos, M.G. (2008). Analysis of Energy Fluxes and Vegetation-Atmosphere Parameters in Irrigated and Natural Ecosystems of Semi-Arid Brazil. Journal of Hydrology 362 (1): 110–27.

Tilman, D., Clark, M. (2014). Global diets link environmental sustainability and human health. Nature, 515(7528): 518-522.

UN (2015). World Population Prospects: The 2015 Revision. Technical report, United Nations, Department of Economic and Social Affairs, Population Division.

UNEP-WCMC (2019). User Manual for the World Database on Protected Areas and world database on other effective area-based conservation measures: 1.6. UNEP-WCMC: Cambridge, UK. Available at: http://wcmc.io/WDPA_Manual

Wada, Y., Wisser, D., Eisner, S., Florke, M., Gerten, D., Haddeland, I., Hanasaki, N., Masaki, Y., Portmann, F.T., Stacke, T., Tessler, Z., Schewe, J. (2013). Multimodel projections and uncertainties of irrigation water demand under climate change. Geophysical Research Letters, 40(17): 4626-4632.

Wagner, W., Hahn, S., Kidd, R., Melzer, T., Bartalis, Z., Hasenauer, S., Figa-Saldaña, J., de Rosnay, P., Jann, A., Schneider, S., Komma, J. (2013). The ASCAT soil moisture product: A review of its specifications, validation results, and emerging applications. Meteorologische Zeitschrift, 22(1), pp.5-33.

Wukelic, G.E., Gibbons, D.E., Martucci, L.M., Foote, H.P., (1989). Radiometric Calibration of Landsat Thematic Mapper Thermal Band. Remote Sensing of Environment 28 (April): 339–347.

V. Appendix General background on SEBAL

116. A satellite does not measure ET fluxes, but spectral radiances that are strongly related to the ET process when properly put into perspective. These spectral measurements are surrogates of the ET process. Because the radiation applies to the moment of overpass time and is aligned with the incoming solar radiation, the satellite measurements can be used to compute an instantaneous ET flux only. The instantaneous ET flux is calculated for each pixel of the image as a "residual" of the surface energy budget equation and is expressed as the energy consumed by the evaporation process (see Figure 27) (Bastianssen et.al, 1998a,b). Indeed a latent heat flux of 28 W/m^2 is equivalent to an evaporation rate of 1 mm/d:

$$LE = Rn - G - H \tag{12}$$

117. Where LE is the latent heat flux (W/m^2), R_n is the net radiation flux at the surface (W/m^2), G is the soil heat flux (W/m^2), and H is the sensible heat flux to the air (W/m^2). LE is converted into ET, expressed as a depth of water per time, by dividing by the latent heat of vaporization and a correction for the density of water. Once the latent heat flux (LE) is computed for each pixel, an equivalent amount of instantaneous ET (mm/s) is readily calculated by dividing by the latent heat of vaporization (L) and the water density (ρ_w):

$$ET = \frac{LE}{L * \rho_w} \tag{13}$$

118. In short, the energy balance approach is an integrative, diagnostic indicator of the overall evaporative status of a discrete patch of land-surface, requiring no *a priori* information of how or why that status evolved.

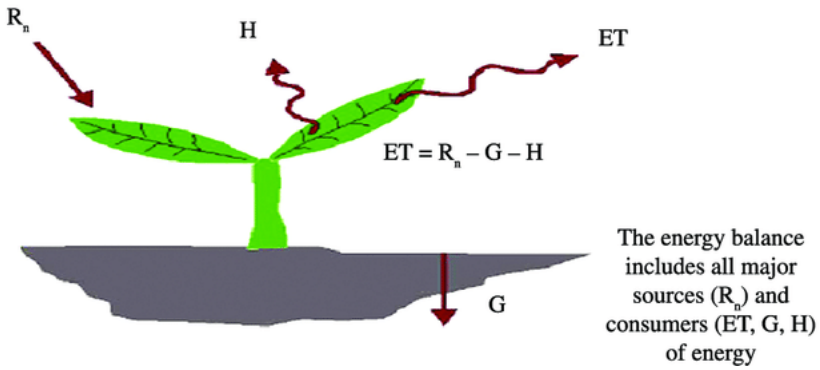

Figure 27 - The components of the Surface Energy Balance. The latent heat flux related to ET is expressed as the residual of the energy balance (adapted after Allen et al.,2012)

119. The net radiation flux (R_n) represents the actual radiant energy available at the surface. It is computed by subtracting all outgoing radiant fluxes from all incoming radiant fluxes (see Figure 28). This is given in the surface radiation balance equation:

$$R_n = R_s^{\downarrow} - \alpha | * R_s^{\downarrow} + R_L^{\downarrow} - R_L^{\uparrow} - (1 - \varepsilon_0) * R_L^{\downarrow} \tag{14}$$

120. Where $R_s^{\downarrow}$ is the incoming shortwave radiation (W/m^2), α is the surface albedo (dimensionless), $R_L^{\downarrow}$ is the incoming longwave radiation (W/m^2), $R_L^{\uparrow}$ is the emitted outgoing longwave radiation (W/m^2), and ε_0 is the surface thermal emissivity (dimensionless). The final term, $(1-\varepsilon_0)R_L^{\downarrow}$, represents the fraction of incoming longwave radiation that is reflected from the surface (see Figure 28).

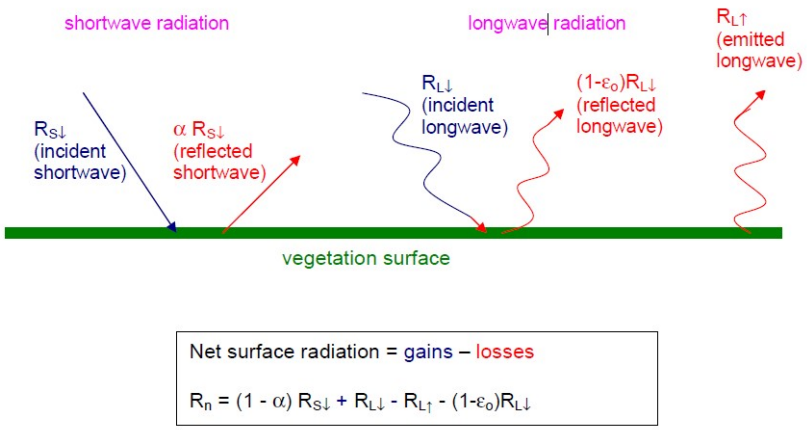

Figure 28 - The components of the Surface Radiation Balance (after Allen et al., 2012)

121. The amount of shortwave radiation ($R_s^{\downarrow}$) that remains available at the surface is a function of the surface albedo (α). Surface albedo is a reflection coefficient defined as the ratio of the broadband reflected radiant flux to the incident radiant flux over the solar spectrum (0.2 to 3.2 μm). It is calculated using satellite image information on spectral radiance for each satellite shortwave band, including visible and near-infrared wavelengths. The incoming shortwave radiation ($R_S^{\downarrow}$) is computed using the solar constant, the solar incidence angle, a relative earth-sun distance, and a computed atmospheric transmissivity. Calculated $R_s^{\downarrow}$ under clear sky conditions are considered to have the same or better accuracy than measured $R_s^{\downarrow}$ from an automated weather station (Allen, 1996; Allen et al., 1998). $R_s^{\downarrow}$ is calculated as a constant for the image time, assuming clear sky conditions (the clear sky is a prerequisite to a useable satellite image), using:

$$R_s^{\downarrow} = G_{sc} * \cos(\phi_{su}) * d_r * \tau_{sw} \quad (15)$$

122. Where: G_{sc} is the solar constant (1367 W/m^2), $\cos(\varphi_{su})$ is the cosine of the solar incidence angle, d_r is the inverse squared relative earth-sun distance, and τ_{sw} is the broad-band atmospheric transmissivity. Values for $R_s^{\downarrow}$ can range from 200 to 1000 W/m^2 depending on the time and location of the image.

123. The incoming longwave radiation ($R_L^{\downarrow}$) is computed using a modified Stefan-Boltzmann equation with atmospheric transmissivity and an air reference temperature. The incoming longwave radiation is the downward thermal radiation flux originating from the atmosphere (W/m^2):

$$R_L^{\downarrow} = \varepsilon_a * \sigma * T_a^4 \quad (16)$$

124. Where: ε_a is the effective atmospheric emissivity (dimensionless), σ is the Stefan-Boltzmann constant (5.67 × 10-8 W/m^2/K^4), and T_a is the near-surface air temperature (K). Outgoing longwave radiation ($R_L^{\uparrow}$) is computed using the Stefan-Boltzmann equation with a

calculated surface emissivity and surface temperature. The emissivity representing surface behaviour for thermal emission in the broad thermal spectrum (6 to 14 μm), expressed as ε_0. The value of ε_0 is used in the calculation of the total longwave radiation emission from the surface L. The outgoing longwave radiation is the thermal radiation flux emitted from the earth's surface to the atmosphere (W/m^2). It is computed by estimating surface thermal emissivity and surface temperature.

$$L^{\uparrow} = \varepsilon_0 * \sigma * T_s^4 \quad (17)$$

125. Vegetation indices are calculated and used to estimate thermal emissivity. The surface emissivity is the ratio of the actual radiation emitted by a surface to that emitted by a black body at the same surface temperature. The emissivity is computed in SEBAL as a function of the Normalized Difference Vegetation Index (NDVI). Three commonly used vegetation indices are computed for each pixel. These are Normalized Difference Vegetation Index (NDVI), Soil Adjusted Vegetation Index (SAVI), and Leaf Area Index (LAI). Anyone of these indices can be used to predict various characteristics of vegetation, depending on the preferences of the user.

$$NDVI = \frac{\rho_5 - \rho_4}{\rho_5 + \rho_4} \quad (18)$$

126. Where ρ_4 and ρ_5 are at-satellite reflectances for Landsat -8 bands 4 and 5. The spectral definitions of Landsat-7 and Landsat-8 are specified in Table 8. Although somewhat similar, their spectral definitions vary. The NDVI is a sensitive indicator of the amount and condition of green vegetation with active chlorophyll. Values for NDVI range between -1 and +1. Green surfaces have an NDVI between about 0.4 and 0.9. Bare soil have often an NDVI ranging between 0 and 0.125. Water bodies, snow, and clouds usually have a value of less than zero. Hence, NDVI is used to filter soil and vegetation (NDVI > 0) from water and snow (NDVI ≤ 0).

127. Surface temperatures are computed from satellite image information on thermal radiance. The surface temperature is computed from the inverse Plank equation for the specific wavelengths of the narrow thermal infrared bands:

$$T_s = K_2 / \ln\left(\frac{\varepsilon_{NB} * K_b}{R_c} + 1\right) \quad (19)$$

128. Where T_s is the surface temperature (K), R_c is the corrected thermal radiance from the surface and K_1 and K_2 are constants for Landsat images. Units for R_c must be the same as those for K_1 ($W/m^2/sr/\mu m$).

Table 7 - Constants K1 and K2 for Landsat.

		K1	K2
		(W/m2/sr/μm)	(K)
Landsat 5	Band 6	607.76	1260.56
Landsat 7	Band 6	666.09	1282.71
Landsat 8	Band 10	774.89	1321.08
Landsat 8	Band 11	480.88	1201.14

129. The Leaf Area Index (LAI) is the ratio of the total area of all leaves on a plant (one side of the leaves) to the ground area represented by the plant and ranges from 0 to 6. LAI is dimensionless (m2/m2) and is an indicator of biomass and canopy resistance to vapour and carbon fluxes. LAI controls the partitioning between soil evaporation and plant transpiration. LAI is computed using various empirical equations.

Table 8 - Spectral definitions of Landsat 7 and 8.

Landsat-7 ETM+ Bands (µm)			Landsat-8 OLI and *TIRS* Bands (µm)		
			30 m Coastal/Aerosol	0.435 - 0.451	Band 1
Band 1	30 m Blue	0.441 - 0.514	30 m Blue	0.452 - 0.512	Band 2
Band 2	30 m Green	0.519 - 0.601	30 m Green	0.533 - 0.590	Band 3
Band 3	30 m Red	0.631 - 0.692	30 m Red	0.636 - 0.673	Band 4
Band 4	30 m NIR	0.772 - 0.898	30 m NIR	0.851 - 0.879	Band 5
Band 5	30 m SWIR-1	1.547 - 1.749	30 m SWIR-1	1.566 - 1.651	Band 6
Band 6	60 m TIR	10.31 - 12.36	*100 m TIR-1*	*10.60 – 11.19*	Band 10
			100 m TIR-2	*11.50 – 12.51*	Band 11
Band 7	30 m SWIR-2	2.064 - 2.345	30 m SWIR-2	2.107 - 2.294	Band 7
Band 8	15 m Pan	0.515 - 0.896	15 m Pan	0.503 - 0.676	Band 8
			30 m Cirrus	1.363 - 1.384	Band 9

130. Eq. (19) showed the relationship between radiation and surface temperature. L6 is measured by the satellite and R_c is the corresponding value at surface level. An atmospheric correction to the thermal radiance from the surface (R_c) is calculated (Wukelic et al. 1989) as:

$$R_c = \frac{L_6 - R_p}{\tau_{NB}} - (1 - \varepsilon_{NB}) * R_{sky} \quad (20)$$

131. Where: L_6 is the spectral radiance of band 6 in Landsat ($W/m^2/sr/\mu m$), R_p is the path radiance in the 10.4 – 12.5 µm band ($W/m^2/sr/\mu m$), R_{sky} is the narrow band downward thermal radiation from a clear sky ($W/m^2/sr/\mu m$), and τ_{NB} is the narrow band transmissivity of air (10.4 – 12.5 µm). Units for R_c are W/m2/sr/µm. The corrected thermal radiance (R_c) represents the actual radiance emitted from the surface whereas L_6 is the radiance that the satellite "sees". In between the surface and the satellite two things occur. First, some of the emitted radiation is absorbed and reflected by the atmosphere (transmissivity) and does not reach the satellite. Second, thermal radiation is emitted by the atmosphere in the direction of the satellite (path radiance) and the satellite "thinks" that this is from the surface.

132. The soil heat flux (G) and sensible heat flux (H) are subtracted from the net radiation flux at the surface (R_n) to compute the "residual" energy available for evapotranspiration (LE). Soil heat flux (G) is empirically calculated using vegetation indices, surface temperature, and surface albedo. Soil heat flux is the rate of heat storage into the soil and vegetation due to conduction. The ratio G/R_n can be estimated using the following empirical equation developed by Bastiaanssen (1995) representing values near midday:

$$G/R_n = T_s * (0.0038 + 0.0074 * \alpha) * (1 - 0.98 * NDVI^4) \quad (21)$$

133. Where T_s is the surface temperature (°C), α is the surface albedo, and NDVI is the Normalized Difference Vegetation Index. G is then calculated by multiplying G/R_n by the value for R_n. Due to the wide spatial variability of G, soil heat flux is a difficult term to evaluate and care should be used in its estimation. The values of G should be checked against actual measurements on the ground. Land classification and soil type will affect the value of G and a soil map is valuable for identifying the various surface types.

134. There are several energy balance models based on thermal remote sensing data, and the essential difference is the specific solution of sensible heat flux (H), as well as the conversion from instantaneous to daily time scales. Sensible heat flux is the rate of heat loss to the air by convection and conduction, due to a temperature difference. It is computed using the following one-dimensional, aerodynamic, temperature gradient based equation for heat transport:

$$H = \frac{\rho_a * c_p * dT}{r_{ah}} \quad (22)$$

135. Where: ρ_a is air density (kg/m^3), c_p is air specific heat (1004 J/kg/K), dT (K) is the vertical air temperature difference ($T_1 - T_2$) between two heights (z_1 and z_2), and r_{ah} is the aerodynamic resistance to heat transport (s/m). Air density is calculated using standard equations for mean atmospheric pressure and the universal gas law taken from Allen et al. (1998) and simplifying for the effect of vapor pressure (virtual temperature is estimated as 1.01 T_s):

$$\rho = \frac{1000P}{1.01(T_s - dT) * R} \quad (23)$$

136. Where: ρ_a is air density (kg/m), P is mean atmospheric pressure, R is the specific gas constant (287 [J kg/K]), T_s is the surface temperature (K) for a pixel, and dT is the near-surface air temperature difference (K).

137. The near-surface air temperature differences (dT) are key in SEBAL for the so-called internal calibration of the energy balance. The range of dT values is assigned between hot and cold pixels such that at the hot pixel LE = 0 W/m^2 applies, and the cold pixel shows H = 0 W/m^2. Hence, the extremes of dT will be fixed in order to force a certain pre-defined range of H. The difficulty, however, is that r_{ah} also varies with the estimate of H. This can be explained by the fact that the mechanical turbulence is enhanced by convection (see Figure 29). The wind speed at a certain height increases if the atmosphere is becoming more stable.

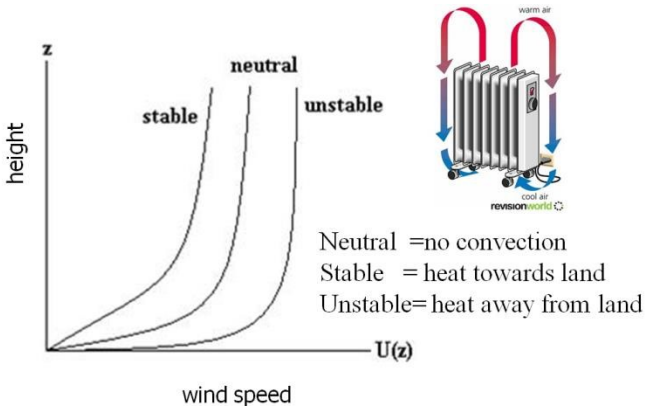

Figure 29 - Impact of convection on increased wind speed and the reduction of the aerodynamic resistance r_{ah}.

138. The buoyancy enhances the turbulence that arises from the mechanical friction between land and the air circulation in the atmosphere. The momentum flux and wind speed simply increase with H. The sensible heat flux (H) is a function of the temperature gradient above the surface, surface roughness, and wind speed. The transfer equation for sensible heat is difficult to solve because there are two unknowns, $r_{ah,}$ and dT. The aerodynamic resistance (and heat transfer) is impacted by the buoyancy of heated, light air at the surface, especially when H is large. Therefore, correction to r_{ah} is needed to account for buoyancy effects. However, H is needed to make this correction. Therefore, an iterative solution for both H and r_{ah} is used. During the first iteration, the aerodynamic resistance to heat transport (r_{ah}) is computed for neutral atmospheric stability conditions as:

$$r_{ah} = \frac{\ln\left(\frac{z_2}{z_1}\right)}{u^* * k} \quad (24)$$

139. Where: z_1 and z_2 are heights in meters above the zero plane displacement (d) of the vegetation, u* is the friction velocity (m/s) which quantifies the turbulent velocity fluctuations in the air, and k is von Karman's constant (0.41). The friction velocity (u*) is computed during the first iteration using the logarithmic wind law for neutral atmospheric conditions:

$$u^* = \frac{k * u_x}{\ln\left(\frac{z_x}{z_{om}}\right)} \quad (25)$$

140. Where: k is von Karman's constant, u_x is the wind speed (m/s) at height z_x, and z_{0m} is the momentum roughness length (m). z_{0m} is a measure of the form drag and skin friction for the layer of air that interacts with the surface. The zero plane displacement (d) and momentum roughness length (z_{0m}) are defined such that the wind speed extrapolates to zero at the height d + z_{0m}. A temperature gradient between two heights both above the surface frees up the calculation of r_{ah} from having to estimate a second aerodynamic roughness for sensible heat transfer (z_{0h}). z_{0h} is difficult to estimate for less than dense vegetation. In addition, surface temperature, T_s, as measured by satellite (i.e., radiometric temperature) can be several degrees different from the "aerodynamic" temperature that drives the heat transfer process (Kustas et al., 1994).

141. The momentum roughness length (z_{0m}) for each pixel can be computed by using (i) a land-use map or (ii) a combined NDVI and surface albedo map. Values for z_{0m} for non-

agricultural surface features (such as water, forest, desert grass, snow, manmade structures, etc.) are generally not well known, and therefore, the operator may wish to use general constant values. When a land-use map is available, z_{0m} for non-agricultural areas can be assigned values. The land use map is essentially an image comprised of specific numbers or values defined to areas representing specific vegetation or type of landform.

142. When a land-use map is not available, a second method for computing the momentum roughness length can be employed (Bastiaanssen, 2000; Teixeira et. al, 2008). In this method, z_{0m} is computed from the following equations:

$$z_{0m} = \exp\left(\frac{a*NDVI}{\alpha} + b\right) \quad (26)$$

143. Where *a* and *b* are regression constants derived from a plot of $\ln(z_{0m})$ vs. NDVI or $\ln(z_{0m})$ vs. NDVI/α for two or more sample pixels representing specific vegetation types. Eq. (26) is an empirical expression that must be fitted to the local vegetation and conditions. The use of albedo (α) to modify NDVI helps to distinguish between some tall and short vegetation types that may have similar NDVI, but different albedo (generally α is lower for taller vegetation due to shading). For example, trees generally have smaller albedo than agricultural crops. To determine *a* and *b* in Eq. (26), a series of sample pixels representing vegetation types and conditions of interest are selected from the respective image and the associated values for NDVI (and surface albedo) are obtained. For each type or condition, a characteristic vegetation height (h) is assigned that represents the specific condition.

144. A series of iterations are required to determine the value for r_{ah} for each period that considers the impacts of instability (i.e., buoyancy) on r_{ah} and H. An initial r_{ah} is computed using Eq. (24) assuming neutral atmospheric conditions. z_1 is the height just above the zero plane displacement for the surface or crop canopy and z_2 is some distance above the zero plane displacement, but below the height of the surface boundary layer. Values of 0.1 m for z_1 and 2.0 m for z_2 are used in SEBAL. z_1 = 0.1 m is assumed to be greater than the aerodynamic roughness length for sensible heat transfer (z_{0h}, where z_{0h} ~ 0.1 z_{0m} ~ 0.01 H) for dense vegetation and z_2 = 2 m is low enough that it can be assumed to be situated in the equilibrium boundary layer above most surfaces, even those of small area extent (Bastiaanssen, 1995).

145. To compute the sensible heat flux (H) from Eq. (22), the near-surface temperature difference (dT) for each pixel needs to be defined. dT is defined as $dT = T_{z1} - T_{z2}$ where T_{z1} and T_{z2} are the air temperatures at heights z_1 and z_2 for any particular pixel. The actual absolute values for air temperatures above each pixel are unknown, including explicit values for T_{z1} and T_{z2}. However, only the difference dT is needed to solve for H and dT has been found to be strongly linear with radiometric surface temperature (Bastiaanssen, 1995). Therefore, dT for each image pixel can be computed by assuming a linear relationship between dT and the DEM corrected value of Ts that is calibrated to each satellite image:

$$dT = a * T_s^{dem} + b \quad (27)$$

146. Where b and a are the calibration coefficients, and T_s^{dem} is surface temperature from the satellite 'delapsed' adjusted to a common sea level datum using a specified lapse rate. The adjustment to T_s compensates for the change in T_s with an elevation that is related more

to warming or cooling of air masses with the change in elevation rather than with a change in surface energy balance and evaporation. T_s^{dem} also includes a correction for the zenith angle as sun-facing pixels (i.e. aspect) and slopes modify the amount of solar radiation received prior to the satellite overpass. Pixels having received larger doses of solar radiation makes them warmer than pixels not having received that extra radiation. A simple cosine zenith angle correction for sloping terrain has been schematized using the instantaneous solar radiation and a thermal slab with heat capacity.

147. To define the a and b coefficients, SEBAL uses the two "anchor" pixels where a value for H can be reliably estimated. These extreme ends of the energy balance need to be picked manually by the user. This brings in a possible bias factor due to subjectivity. It is known that different SEBAL users may come with different values for a and b. Values for H and dT at these "anchor" pixels ought to be computed manually. The linearity of the dT vs. T_s^{dem} function is a major assumption of SEBAL and is essentially the core of the model that forces the partitioning of R_n into H and LE to be correct at the endpoints (Bastiaanssen, 1995).

148. The development of the dT vs. T_s^{dem} equation is as follows: At the "cold" pixel, we define H = 0 W/m^2. SEBAL is to choose the temperature for the "cold" pixel as that from a body of water in the image where one assumes that at this temperature (T_s for the water body) H = 0 W/m^2; and therefore dT_{cold} = 0 K. Since not every image holds a water body, the same type of computation can also be applied to moist dense vegetation (e.g. irrigated crop or a vegetated wetland pixel). The "nearly coldest" (wet) agricultural fields in a satellite image (when at the full cover (LAI > 4)) have H rates that are fluctuating between -50 to + 50 W/m^2.

149. When viewing a large population of fields, a specific sub-population of fields will have somewhat wetter conditions and a slightly cooler temperature than the "mean water body temperature".

150. At the "hot" pixel, $H^{hot} = R_n - G$ applies. ET^{hot} is assumed to be zero or nearly zero for a "hot" (dry) agricultural field having no green vegetation and with dry soil surface layer. The weather data should be checked to see if this assumption is correct. H^{hot} for the hot pixel is calculated from:

$$dT^{hot} = H^{hot} * \frac{r_{ah}^{hot}}{\rho_a * c_p} \quad (28)$$

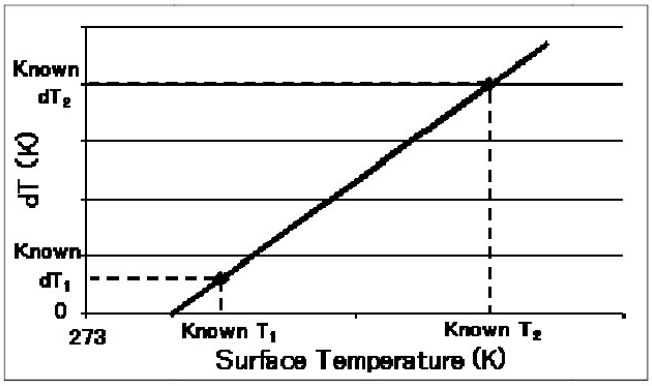

Figure 30 - Linear function between dT and surface temperature points (different values of T_s^{dem}).

151. The temperature difference (dT) for each pixel can now be computed in the image processing model using the coefficients b and a and the surface temperature (T_s DEM of each pixel).

152. SEBAL applies the Monin-Obukhov theory in an iterative process (see Figure 31). Atmospheric conditions of stability have a large effect on the aerodynamic resistance (r_{ah}) and must be considered in the computation of sensible heat flux (H), especially for dry conditions. SEBAL repeats the computation of H through a number of iterations, each one correcting for buoyancy effects until the value for r_{ah} stabilizes. Stabilization usually occurs after four or five iterations.

153. The Monin-Obukhov length (L) is used to define the stability conditions of the atmosphere in the iterative process. L is the height at which forces of buoyancy (or lack of) and mechanical mixing are equal. If L < 0, the atmosphere is considered unstable; if L > 0, the atmosphere is considered stable. It is calculated as a function of the heat and momentum fluxes:

$$L = -\frac{\rho_a * c_p * u^{*3} * T_s}{k * g * H} \quad (29)$$

154. Where: ρ_a is the density of air (kg/m3), c_p is the air specific heat (1004 J/kg/K), u* is the friction velocity (m/s), T_s is the surface temperature (K), g is the gravitational constant (9.81 m/s^2), and H is the sensible heat flux (W/m^2). Values for L define the stability conditions of the atmosphere.

155. With first estimates of u* and r_{ah} available, it becomes feasible to compute H for every pixel. This estimate for H can be used to describe the convection. The presence of convection increases u* which will make the transfer of heat more efficiently. This implicit H - u* - r_{ah} - H chain requires a number of iterations before it stabilizes (see Figure 5).

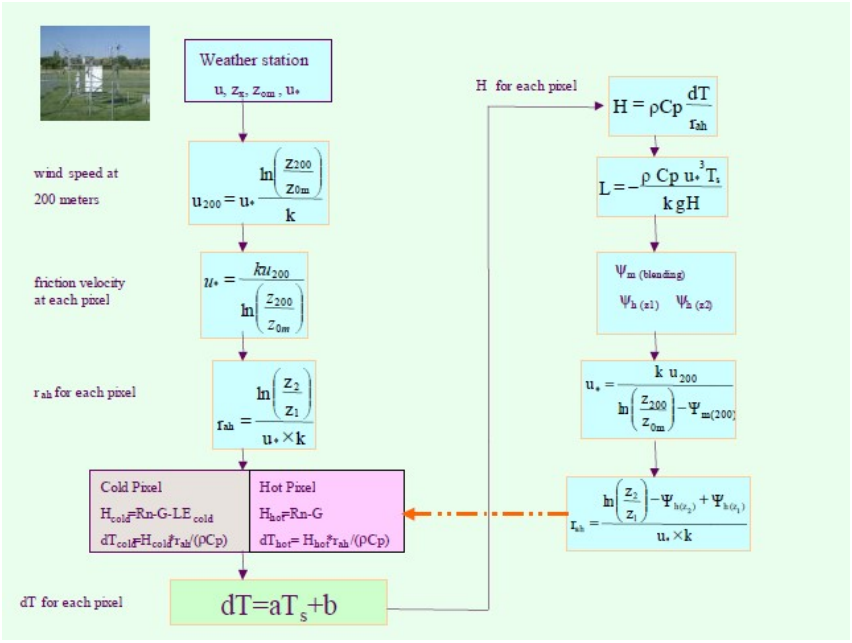

Figure 31 - Flow Chart of the Iterative Process for the Calculation of Sensible Heat (H).

156. The upscaling from the instantaneous to daily surface energy balance is done by means of the evaporative fraction. The instantaneous evaporative fraction EF_i is defined as:

$$EF_i = \frac{LE}{R_n - G} \tag{30}$$

157. The value of EF_i is rather conserved with time because R_n and LE follow the same solar-related parabolic shape during the daytime cycle. This results in a quasi-constant graph of EF_i, especially during midday hours (Shuttleworth et al., 1989; Bastiaanssen et al., 1996; Dos Santos et al., 2010).

158. SEBAL is converting EF_i into a 24-hour counterpart EF_{24} by means of an advection factor Ω that depends on the vapor pressure deficit and aims at describing the increase of EF_i during the afternoon. An advection factor Ω is introduced to make a correction:

$$EF_{24} = \Omega * EF_i \tag{31}$$

Where

$$\Omega = 1 + 0.985 * EF_i \left(\exp\left((e_{sat}^{24} - e_{act}^{24}) * 0.08\right) - 1.0\right) \tag{32}$$

So that finally, the 24 hours averaged latent heat flux can be obtained:

$$LE_{24} = EF_{24} * (Rn_{24} - G_{24}) \tag{33}$$

159. Due to the heating of the topsoil during daytime and cooling during night time, the 24-hour version of the soil heat flux (G_{24}) is negligibly small. It is convenient to reduce Eq. (33) into:

$$LE_{24} = EF_{24} * R_{n_{24}} \tag{34}$$

160. Note that LE_{24} is input into Eq. (13) for determining the daily evapotranspiration rate (mm/d). The net radiation can be computed from the 24 hours averaged net shortwave solar radiation and a simple correction term for net longwave radiation. The standard equations required to get the 24 hours averaged incoming solar radiation are described in FAO56 (Allen et al., 1998).

$$R_{n_{24}} = (1 - \alpha) * K_{24}^{\downarrow} - L_{net} \quad (35)$$